



# Recent strategies for constructing efficient interfacial solar evaporation systems

Yida Wang<sup>1,3</sup>, Junqing Hu<sup>2</sup>, Li Yu<sup>2</sup> (✉), Xuan Wu<sup>3</sup>, Yingying Zhang<sup>1</sup> (✉), and Haolan Xu<sup>3</sup> (✉)

<sup>1</sup> Key Laboratory of Organic Optoelectronics and Molecular Engineering of the Ministry of Education, Department of Chemistry, Tsinghua University, Beijing 100084, China

<sup>2</sup> College of Health Science and Environmental Engineering, Shenzhen Technology University, Shenzhen 518118, China

<sup>3</sup> Future Industries Institute, UniSA STEM, University of South Australia, Mawson Lakes Campus, SA 5095, Australia

Received: 23 January 2023 / Revised: 12 February 2023 / Accepted: 23 February 2023

## ABSTRACT

Interfacial solar evaporation (ISE) is a promising technology to relieve worldwide freshwater shortages owing to its high energy conversion efficiency and environmentally sustainable potential. So far, many innovative materials and evaporators have been proposed and applied in ISE to enable highly controllable and efficient solar-to-thermal energy conversion. With rational design, solar evaporators can achieve excellent energy management for lowering energy loss, harvesting extra energy, and efficiently utilizing energy in the system to improve freshwater production. Beyond that, a strategy of reducing water vaporization enthalpy by introducing molecular engineering for water-state regulation has also been demonstrated as an effective approach to boost ISE. Based on these, this article discusses the energy nexus in two-dimensional (2D) and three-dimensional (3D) evaporators separately and reviews the strategies for design and fabrication of highly efficient ISE systems. The summarized work offers significant perspectives for guiding the future design of ISE systems with efficient energy management, which pave pathways for practical applications.

## KEYWORDS

interfacial solar evaporation, photothermal materials, energy management, molecular engineering

## 1 Introduction

Freshwater scarcity has become one of the most critical global issues endangering the long-term sustainability of human society [1–6]. To mitigate this problem, in recent years, great efforts have been devoted to developing desalination technologies to produce clean water from seawater [7–9]. While the two traditionally used desalination technologies have been membrane filtration and thermal distillation, neither of these approaches has met the desired high level of environmental friendliness because they both consume intensive amounts of electricity derived from fossil fuels [10–13]. Therefore, new desalination technologies driven by green and sustainable energy sources are currently in high demand [14, 15]. Interfacial solar evaporation (ISE) driven desalination is a promising solution for environmentally friendly and sustainable freshwater production [15, 16].

ISE process involves efficient solar light-to-heat conversion and heat localization at evaporation surfaces to enhance water evaporation [17]. Therefore, compared to conventional bulk heating solar distillation, ISE technologies exhibit outstanding solar-to-vapor energy conversion efficiency. Rational structure design of photothermal evaporators and judicious energy management of ISE allow converted heat from sunlight to be

localized at the evaporation surface for efficient vapor generation instead of dissipation into the environment. The recent progress and evolution of ISE technology have primarily been facilitated by optimization of energy management [18]. Photothermal materials and evaporator design were optimized and elaborated towards more efficient energy utilization, via (1) minimizing energy loss from evaporation system to the ambient environment; (2) extending energy input from the ambient environment to enhance evaporative contributions; (3) reducing evaporation enthalpy to realize more efficient vaporization processes.

This review systematically summarizes these pathways for enhancing practical solar evaporation performance (Fig. 1). It introduces the energy nexus in two-dimensional (2D) and three-dimensional (3D) evaporation systems and points out the main differences. It is clearly demonstrated that the evaporation rate can be significantly enhanced by either applying materials with highly efficient light-to-heat conversion or structure design of state-of-art evaporators with smart energy management strategies. This review also summarizes the reduction in water vaporization enthalpy by molecular engineering, such as surface functional group modulation and hierarchical structure design. These significant findings have paved the way for new design of interfacial solar

© The Author(s) 2023. Published by Tsinghua University Press. The articles published in this open access journal are distributed under the terms of the Creative Commons Attribution 4.0 International License (<http://creativecommons.org/licenses/by/4.0/>), which permits use, distribution and reproduction in any medium, provided the original work is properly cited.

Address correspondence to Li Yu, [yuli@sztu.edu.cn](mailto:yuli@sztu.edu.cn); Yingying Zhang, [yingyingzhang@tsinghua.edu.cn](mailto:yingyingzhang@tsinghua.edu.cn); Haolan Xu, [haolan.xu@unisa.edu.au](mailto:haolan.xu@unisa.edu.au)

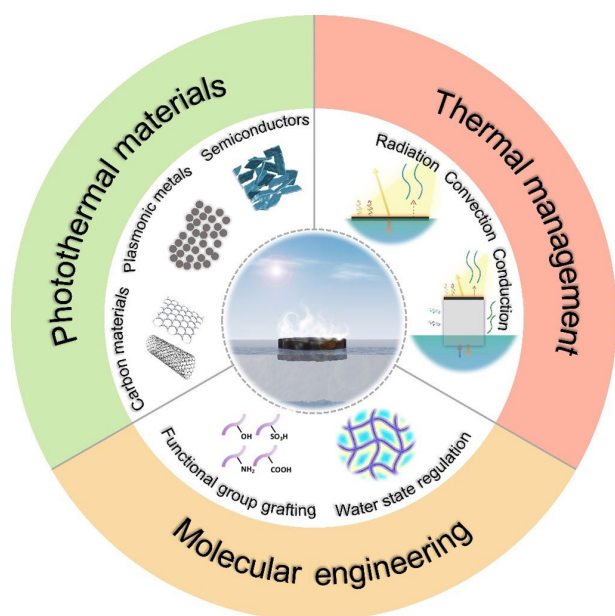


**Figure 1** Schematic diagram of strategies for constructing efficient ISE systems.

evaporators to optimize the energy nexus by considering both photothermal materials, energy nexus, and all environmental factors during solar evaporation. The reviewed strategies thus may provide valuable guides for achieving high-performance ISE for practical applications.

## 2 Highly efficient solar absorbers

Solar absorbers play a critical role in overall solar energy conversion. The light-to-heat conversion efficiency directly determines the amount of solar energy available for ISE. In recent years, owing to the rapid development in materials science and nanotechnology, various types of materials have been synthesized and demonstrated excellent light-to-heat conversion efficiency. The three main types of photothermal materials intensively used as solar absorber in ISE systems are plasmonic metals, semiconductors, and carbon-based materials [19–35]. Since a number of review articles have focused on photothermal materials for ISE, we herein only briefly introduce these three types of solar absorbers.

### 2.1 Plasmonic metals

Metal materials which exhibit plasmonic effects have often been used as solar absorbing materials [36–40]. These plasmonic metals have their own inherent oscillation frequency of free electrons, so that once incident photons of a specific frequency reach the metal surfaces, a near field-electron enhancement will be achieved with a

matching frequency for that metal (Fig. 2(a)), which is known as surface plasmon resonance (SPR) effect. Under resonant illumination by incident light, the plasmon-excited electrons are non-radiatively damped via the Landau damping mechanism and redistribute their energy through electron–electron and electron–phonon scattering processes to generate heat. Owing to this plasmon resonance, the light-to-heat conversion efficiency can be easily boosted to > 95%. Currently, plasmonic metals, such as gold [36, 41], silver [42], copper [43, 44], cobalt [45], aluminium [46], and indium [39] have all been utilized as photothermal materials. Due to the good stability of noble metals, they are applicable under extreme conditions. However, one major drawback of noble metals is the extremely high cost, which limits their large-scale practical applications.

### 2.2 Semiconductors

Low cost and low toxicity semiconductors have emerged as a potential choice of solar absorber [47–64]. Under solar irradiation, electron–hole pairs are generated in semiconductors when the light energy is higher than the bandgap (Fig. 2(b)). For narrow bandgap semiconductors, when the excited electron–hole pairs return to the band edges, they will release extra energy as heat. While for broadband semiconductors, the light energy is mostly utilized to re-emit photons but not heat. Recently, several semiconductors have been developed as solar absorbers, including titanium- and molybdenum-based semiconductors [65–72], NiO [61, 63, 73], CuO [74–76],  $\text{Cu}_x\text{S}_y$  [77–79],  $\text{CoWO}_{4-x}$  [80],  $\text{Fe}_3\text{O}_4$  [81, 82], and MXene [29, 34, 83–91]. Despite showing great potential for efficient light-to-heat conversion, the relatively low stability of some semiconductors has hindered their further growth for practical ISE applications.

### 2.3 Carbon-based materials

Carbon-based materials are naturally black which renders the materials superior performance in receiving broad-band solar light [92–104]. More than half of the reported works in the field of ISE utilized carbon-based materials as solar absorbers. The process of light-to-heat conversion in carbon-based materials involves excitation of electrons by solar irradiation and their subsequent relaxation to the ground state. With rapid lattice vibration (Fig. 2(c)), the solar radiation energy is quickly thermalized on the surfaces. So far, carbon-based materials including carbon black [105], graphite [106], carbon nanotube [61, 107–112], graphene oxide [113–115], reduced graphene oxide [114–120], and various polymers [27, 121–132] have been used as solar absorbers. The low cost and natural accessibility of such carbon-based materials make them prime candidates for practical ISE. Additionally, these materials typically exhibit excellent chemical and physical stability, placing carbon-based materials in a unique position for large-scale and practical applications.

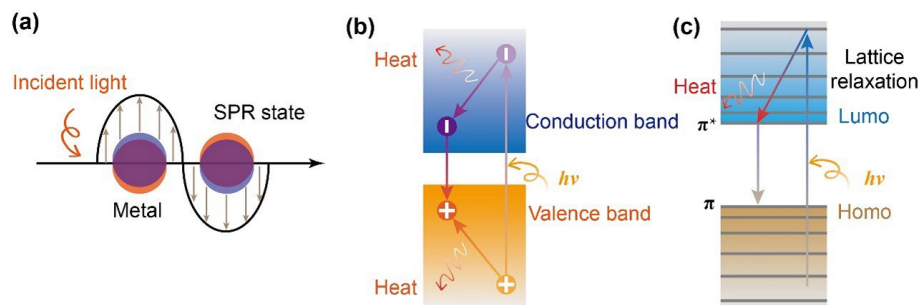


**Figure 2** Photothermal conversion mechanisms of (a) plasmonic metals, (b) semiconductors, and (c) carbon-based materials.

### 3 Highly efficient energy management in 2D ISE systems

In part, due to the extensive exploration and evaluation of different photothermal materials, ISE systems with general 2D evaporators have been widely reported. There is no doubt that solar absorbers with excellent light absorption can realize maximum solar energy input. However, if the system lacks rational energy management, a considerable fraction of generated thermal energy will be directly lost and not be utilized for water evaporation. Therefore, optimization of energy management during solar evaporation is extremely important for achieving high energy efficiency.

In a typical 2D ISE system, the energy nexus during solar steam generation is depicted in Fig. 3. The photothermal layer absorbs and converts the incident solar light ( $P_{\text{solar}}$ ) into heat for vapor generation ( $P_{\text{vapor}}$ ). During this process, part of the light is scattered and reflected from the surface to the ambient environment, inducing a loss in solar energy harvesting ( $P_{\text{reflection}}$ ). Most of the converted heat is consumed by water evaporation, while the surplus heat on the evaporation surface gives rise to a higher surface temperature than that of the surrounding ambient air and bulk water. Therefore, radiative ( $P_{\text{radiation}}$ ) and convective ( $P_{\text{convection}}$ ) thermal losses from the evaporation surface to the ambient environment occur due to this temperature difference. In addition, conductive heat loss ( $P_{\text{conduction}}$ ) from the evaporation surface to the bulk water also occurs. The ISE system also contains additional energies that are not derived from direct solar light. This includes the latent heat released from vapor condensation, which is discharged when the generated hot vapor encounters cold air above the evaporation surface. In a 2D ISE system, the energy transfer process does not always involve latent heat, since it is often hard to recycle this part of the energy by the 2D evaporation surface located under the latent heat releasing zone. Therefore, the energy nexus for a 2D ISE system can be described using Eq. (1)

$$P_{\text{solar}} = P_{\text{vapor}} + P_{\text{reflection}} + P_{\text{radiation}} + P_{\text{convection}} + P_{\text{conduction}} \quad (1)$$

The solar energy input  $P_{\text{solar}}$  can then be calculated based on light absorption and reflection using Eqs. (2) and (3), respectively

$$P_{\text{solar}} = AE_{\text{in}} \quad (2)$$

$$P_{\text{reflection}} = A(1 - \alpha)E_{\text{in}} \quad (3)$$

where  $A$ ,  $E_{\text{in}}$ , and  $\alpha$  represent the area of solar evaporation surface (SES), the energy of the incident light ( $1.0 \text{ kW}\cdot\text{m}^{-2}$  for 1 sun), and the optical absorption coefficient (generally noted as the absorbance from 200 to 2500 nm), respectively.

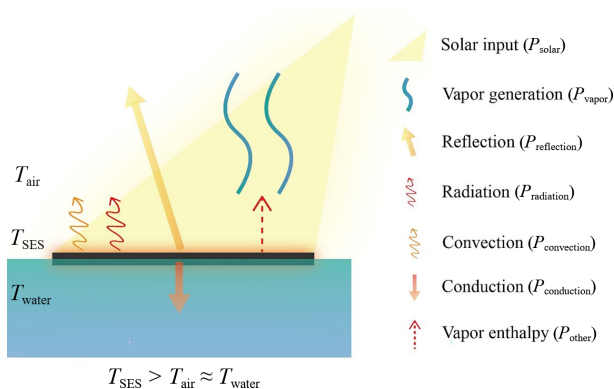


**Figure 3** Schematic illustration of the energy nexus in a typical 2D ISE system.

The radiative and convective energy losses are calculated via Eqs. (4) and (5) as shown below

$$P_{\text{radiation}} = A\varepsilon\sigma(T_1^4 - T_0^4) \quad (4)$$

$$P_{\text{convection}} = Ah(T_1 - T_0) \quad (5)$$

where  $\varepsilon$  is the emissivity of the evaporation surface and  $\sigma$  is the Stefan–Boltzmann constant ( $5.67 \times 10^{-8} \text{ W}\cdot\text{m}^{-2}\cdot\text{K}^{-4}$ ).  $h$  represents the convection heat transfer coefficient (generally from 5 to  $10 \text{ W}\cdot\text{m}^{-2}\cdot\text{K}^{-1}$  for interfacial evaporation).  $T_0$  and  $T_1$  are the ambient and evaporation surface temperatures during solar evaporation.

The conductive heat loss from the evaporation surface to the bulk water can be expressed by Eq. (6)

$$P_{\text{conduction}} = -Cm\Delta T \quad (6)$$

where  $C$  is heat capacity of the water,  $m$  is the mass of bulk water, and  $\Delta T$  is the temperature difference of the bulk water during solar evaporation.

Based on the gradual understanding of the energy nexus in 2D ISE system, the strategies towards efficient solar energy utilization for water evaporation were demonstrated in recent years. The principle is noted as promoting energy harvest from the incident solar light while minimizing the energy loss from the ISE system to the environment.

#### 3.1 Minimizing solar reflection

As depicted in Eqs. (2) and (3), the efficient utilization of solar light requires to reduce solar reflection on the absorber surface. The reflectance of the solar absorber is normally related to its surface morphology. If the surface of solar absorber is flat without sub-structures, a part of the incident light is directly reflected from the surface. In contrast, the surface with hierarchical structures enables multiple reflections of the incident solar light and eventually results in light extinction. Therefore, an efficient initiative of reducing solar reflection requires morphology and structure tailoring of the absorber surface [133–141]. The previous work reported several typical strategies in this regard [142–145], as illustrated in Figs. 4(a)–4(d). The first one [142] reported a hierarchical structure constructed by grafting graphene sheets onto the 3D porous polyvinyl alcohol (PVA) networks (Fig. 4(a)). In addition to the solar conversion, the graphene sheets with random distribution also increased the specific surface area for multiple reflections. The incident light was trapped in the porous networks with the assistance of graphene sheets attachment. The solar reflectance was thus decreased accordingly. Another strategy [143] for minimizing solar reflection is to stack the crumpled layers in horizontal alignment (Fig. 4(b)). The presence of the layer-by-layer structure facilitated light dissipation between layers which was considered as a strong complement to the solar reflection on the top rough surface. Additionally, some very similar structures with vertically aligned layers were demonstrated to be very effective in reducing solar reflection, such as the structural design [144] shown in Fig. 4(c). It applied CuO nanowires as skeleton and graphdiyne (GDY) as solar absorbing material. The high specific surface area of GDY integrating with CuO nanowire forest benefited multiple solar reflection processes in the internal gaps. An outstanding solar absorption enhancement was thus realized. Moreover, some recent work adopted laser writing to engrave the surface patterns for fully receiving incident solar light. As depicted in Fig. 4(d), the surface

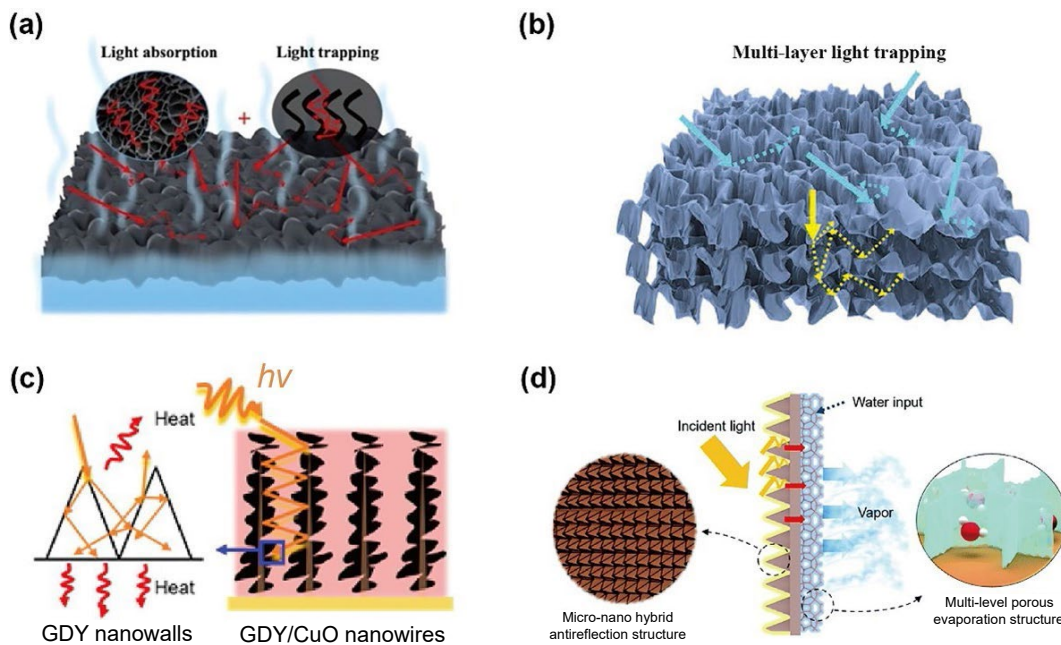


**Figure 4** (a) Schematic illustration of reducing solar reflectance by rough surface light trapping. Reproduced with permission from Ref. [142], © Tsinghua University Press and Springer-Verlag GmbH Germany, part of Springer Nature 2020. (b) Proposed mechanism of multi-layer light trapping to reduce reflectance. Reproduced with permission from Ref. [143], © WILEY-VCH Verlag GmbH & Co. KGaA, Weinheim 2019. (c) Hierarchical surface structure enabled avoidance of solar reflection. Reproduced with permission from Ref. [144], © American Chemical Society 2017. (d) Tailoring surface pattern of solar absorbing layer for lowering reflection. Reproduced with permission from Ref. [145], © The Royal Society of Chemistry 2021.

was tailored into the triangular grooves by laser treatment [145]. The patterned surface enabled minimizing solar reflection from different incident angles. The incident solar light was mostly confined in the grooves until being absorbed. All these efforts pave the way for centering highly efficient solar absorption processes by suppressing solar reflection on evaporation surfaces.

### 3.2 Minimizing radiative and convective heat losses

In addition to mitigating reflective solar energy loss, some subsequent research work focused on avoiding radiation and convection losses from the evaporation surface to the surrounding air [146–151]. As depicted in Eq. (4), thermal radiation loss is mainly caused by the high emissivity of photothermal evaporation surface and its higher surface temperature compared to the surrounding air, resulting in a net flux of infrared (IR) photons being emitted to the ambient environment. Therefore, an efficient suppression of radiation loss can be realized by lowering the emissivity of the photothermal materials and evaporation surface temperature. Accordingly, a dual-layer design [149] was applied for reducing the radiative loss (Fig. 5(a)(i)). In this work, Ni nanoparticles (NPs) were encapsulated in carbon and silica shells and assembled in an orderly manner to form a solar harvesting structure of graded refractive indices on an infrared reflector (Fig. 5(a)(ii)). With the design of the infrared reflecting module, the solar absorber realized low thermal emittance so that the radiative loss was successfully reduced (Fig. 5(a)(iii)).

According to the thermodynamics, convection is more complicated than radiation. For temperature difference  $< 50$  K, Eq. (5) (Newton's law) is valid for expressing the convection process, where the convective heat loss depends on the convection coefficient and the temperature difference between the evaporation surface and the surrounding environment. However, during solar evaporation, convection loss is normally simultaneously accompanied by radiative loss. Convection is regarded as a hybrid thermal transfer effect, so very little work

manipulated convective issue independently. Complexities also exist in the nature of the ambient fluid (liquid or gas), the physical parameters of the fluid (mass density, thermal conductivity, specific heat capacity, and dynamic viscosity), and the geometric and physical properties of the evaporation surface (hydrophilicity, microstructures, surface roughness, and water content). Although many factors need to be considered to comprehensively understand the mechanism of heat convection, there are still regularities to follow.

As depicted in Eq. (5), reducing the affordable area of the surrounding fluid would logically reduce convection loss, which could be enabled by partially covering the interface between evaporation layer and the air (Fig. 5(b)(i)). This work [150] demonstrated an unconventional cup-shape design for ISE process. During solar evaporation, the generated vapor escaped from the bottom layer of the absorber and condensed at the wall of a copper-based cup (Fig. 5(b)(ii)). Due to the unique downward vapor collecting approach, the photothermal evaporation surface was allowed to be covered by a protective layer (Fig. 5(b)(iii)). The covered layer enabled a convection free zone above the evaporation surface which eliminated the convective loss from the ISE system to the surrounding air. In addition, the air convection above the evaporation surface spontaneously induced by solar evaporation could be regulated by surface tailoring [151]. Xu's group reported that with the increase in the size of the evaporation surface, the evaporation rate decreased. The reason is that the middle portion of the large evaporation surface acts as a "dead evaporation zone" with little contribution to vapor generation during solar evaporation. As depicted in Fig. 5(c)(i), the intensity of air convection above the middle evaporation surface was much lower than that at the edges which indicated the middle portion of the evaporation surface had vapor accumulation and was not active in water evaporation. When the middle portion of the evaporation surface was selectively removed, although the total evaporation surface area decreased, both the evaporation rate and

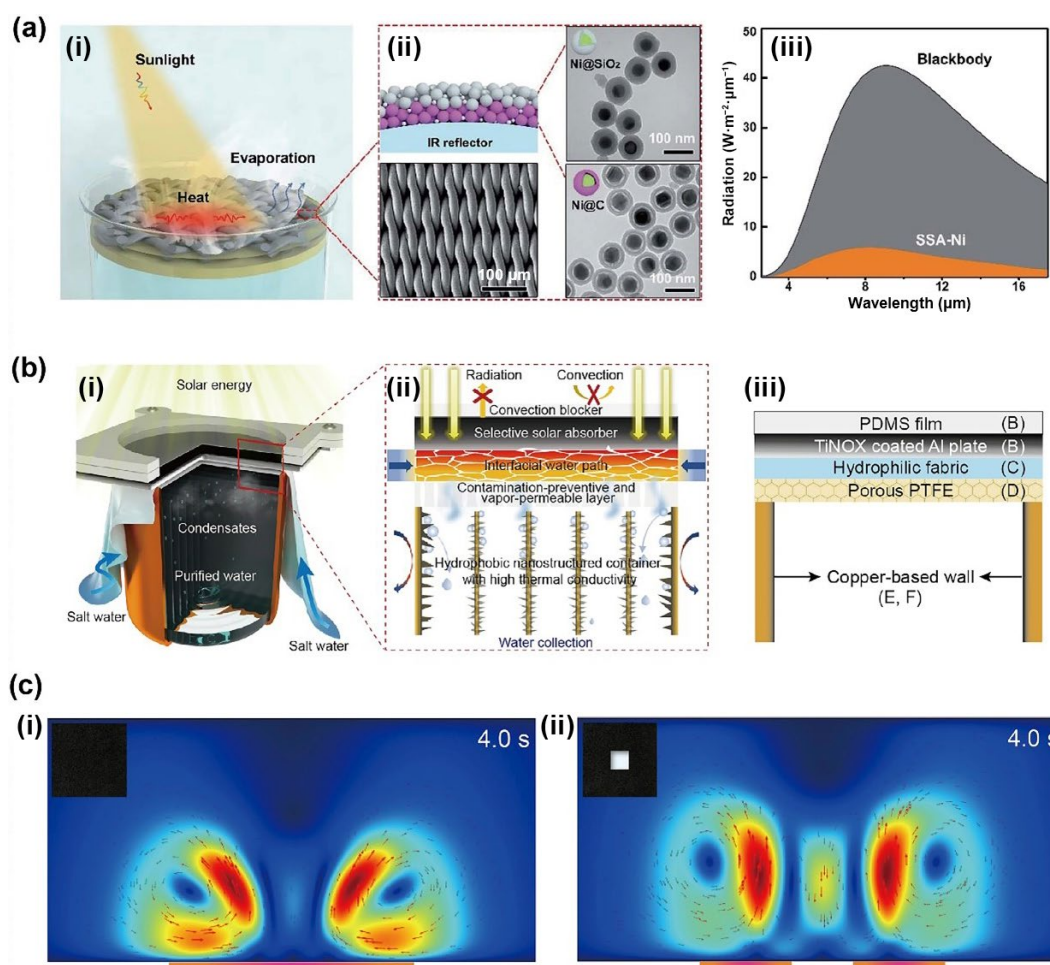


**Figure 5** (a) Concentrating converted heat for evaporation via minimizing interfacial radiation loss: (i) schematic illustration, (ii) microscopic images of as-fabricated selective solar absorber, and (iii) radiative flux nexus of the selective solar absorber in infrared range. Reproduced with permission from Ref. [149], © The Royal Society of Chemistry 2021. (b) Highly efficient utilization of converted heat for evaporation via minimizing interfacial convection loss: (i) set-up diagram of the cup-shape water purification system, (ii) schematic illustration of the process of solar water purification, and (iii) diagram of specific configuration of the solar water purification system that contained convective flow protection layer. Reproduced with permission from Ref. [150], © Elsevier Inc. 2021. (c) Tailoring evaporation surface for convective activation: (i) numerical simulation of air convection above an 8 cm × 8 cm evaporation surface (left corner) during solar evaporation and (ii) simulated convection above an 8 cm × 8 cm evaporation surface with a 2 cm × 2 cm area removed from the middle (left corner) during solar evaporation. Reproduced with permission from Ref. [151], © Science China Press 2022. Published by Elsevier B.V. and Science China Press.

vapor output increased due to the reconfigured and enhanced convection above the entire evaporation surface (Fig. 5(c)(ii)). Therefore, it demonstrated that the regulation of air convection by surface topology design is also a promising strategy for evaporation rate enhancement in interfacial solar evaporation systems.

### 3.3 Minimizing conductive heat loss

The water pathway is one of the key components in an ISE system. A rational water pathway ensures an adequate water supply and simultaneously localizes heat on the evaporation surface during solar evaporation. Advances in constructing an efficient ISE system require smart water pathway designs. To date, water transport structures have evolved in three main types from a self-floating 3D water path (i.e., full contact between the evaporation surface and bulk water) to the water paths in 2D and one-dimensional (1D) forms (Fig. 6).

The initial proposed evaporator designs involved floating photothermal materials on the bulk water surface [152–168]. Normally, in this case, the selected materials are porous and lightweight to ensure self-floating and adequate water supply.

During solar evaporation, water would be pumped from the bulk water to the top evaporation surface through capillary force. Although the full contact between such materials and the bulk water can give continuous water supply, it also leads to more energy loss from the evaporation surface to the bulk water by heat conduction during solar evaporation. The typical 3D water path [161] for interfacial solar evaporation was demonstrated in Fig. 6(a)(i), where the porous melamine foam was employed as solar evaporator (Fig. 6(a)(ii)). The interconnected channels of the foam could sustain water flow from the bottom to the evaporation surface via capillary force. Since the water flowing path was not further regulated, the conductive heat directly transferred to the underneath bulk water through the pores of the foam. In this regard, the normal strategy to reduce conductive heat loss is to increase the thickness of the evaporator (i.e., lengthening the water paths).

Recently, the water path designs were developed towards more efficient energy management for evaporation, which could be mainly classified as 2D and 1D water paths (Figs. 6(b) and 6(c)). Evaporators with 2D water path demonstrated efficient evaporation performance by using light-weight thermal insulation

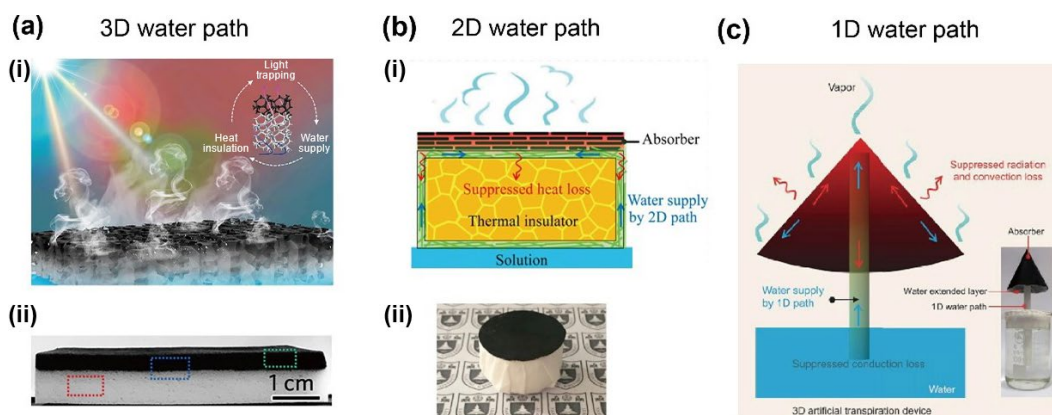


**Figure 6** (a) Typical 3D water path of ISE system: (i) diagram of interconnected water transportation and solar evaporation processes by using a melamine-foam-based evaporator and (ii) the photograph of the melamine-foam-based evaporator with 3D interconnected water path. Reproduced with permission from Ref. [161], © American Chemical Society 2020. (b) Typical 2D water path of ISE system: (i) schematic illustration of 2D water path by using a PS foam thermal insulator as a support and (ii) the photograph of the solar evaporator with 2D water path. Reproduced with permission from Ref. [170], © Li, X. Q. et al. 2016. (c) An umbrella-shaped solar evaporator with 1D water path. Reproduced with permission from Ref. [177], © Li, X. Q. et al. 2017.

foam warped by a thin and confined water transportation layer [81–87, 102, 169–172]. For example, a polystyrene (PS) foam thermal insulator was configured at the bottom of the solar absorber (Figs. 6(b)(i) and 6(b)(ii)) [170]. Only a small part of the materials containing water was immersed in the bulk water instead of full contact. During solar evaporation, the conductive heat transfer paths corresponded to the water flowing paths. The decreased contact area led to lower heat exchange between the evaporation surface and the bulk water. Therefore, the conductive energy loss to bulk water was further suppressed and more efficient heat localization was achieved via this 2D water path design. Additionally, some work reported more efficient designs with one narrow water path [173–178]. As illustrated in Fig. 6(c), similar to evaporators with a 2D water paths, this approach [177] had very good thermal management where only a narrow 1D heat conduction path was used to avoid conductive heat loss. With further optimization of the 1D path length, the heat conduction loss from the evaporation surface to the bulk water was eliminated by this umbrella design. Owing to the advanced energy management in heat conduction, it realized the improved solar-to-vapor efficiency.

#### 4 Highly efficient energy management in 3D systems

Recently, a paradigm shift occurred in our understanding of energy management in 3D solar evaporators, which has subsequently affected most 3D evaporator designs. In 3D evaporators, the newly developed strategy is to expand energy input options for ISE, by harvesting extra energy from the surrounding environment together with solar energy input [179]. Figure 7 illustrates the mechanism of obtaining environmental energy using a 3D ISE design and the energy transfer process during solar evaporation.

Unlike a 2D structure where solar light is absorbed on the entire evaporation surfaces, 3D evaporators have additional surfaces that are not exposed to solar light. Taking a 3D cylindrical evaporator as example, during solar evaporation, the top evaporation surface as SES receives light ( $P_{\text{solar}}$ ) and generates vapor ( $P_{\text{solar vapor}}$ ). The light-to-heat conversion on this surface induces higher surface temperature and the consequent energy loss to the ambient environment via reflection ( $P_{\text{reflection}}$ ), radiation ( $P_{\text{radiative loss}}$ ), and convection ( $P_{\text{convective loss}}$ ). There is also a downward

conductive heat loss ( $P_{\text{conduction}}$ ) to the bulk water due to the temperature difference between SES and the water body. In this way, solar evaporation on SES is similar to the energy transfer process in 2D systems. However, the evaporation on the surfaces without solar irradiation (cold evaporation surface (CES)) is quite different from that in 2D systems. The side walls of the 3D evaporator cannot receive solar light directly so that a cold evaporation (i.e., dark evaporation) occurs ( $P_{\text{cold vapor}}$ ). The evaporative cooling effect gives rise to the lower surface temperature on CES than the ambient temperature. Based on thermodynamic laws (Eqs. (4) and (5)), a reversed energy flow from the surrounding air to the evaporation surfaces via radiation and convection ( $P_{\text{radiative gain}}$  and  $P_{\text{convective gain}}$ ) occurs. This passive energy harvest resulted in more energy sources being available for water evaporation, which could break the theoretical limit assuming 100% light-to-vapor energy conversion. Based on the above analysis, the energy nexus in this 3D ISE system is expressed by Eq. (7)

$$P_{\text{solar}} + P_{\text{radiative gain}} + P_{\text{convective gain}} = P_{\text{solar vapor}} + P_{\text{cold vapor}} + P_{\text{reflection}} + P_{\text{radiative loss}} + P_{\text{convective loss}} + P_{\text{conduction}} \quad (7)$$

This equation highlights possible strategies for achieving highly efficient evaporation performance in 3D ISE systems. The principal point is to create additional CESs in confined space (i.e., occupied area) in order to gain as much energy as possible from the surroundings in addition to the solar light energy. Other strategies guiding research in this area include reducing, eliminating, or even reversing energy loss to the surroundings and the bulk water through 3D evaporator designs. Moreover, using convective flow or other energy sources to assist solar evaporation is also considered to improve water evaporation performances, which has been demonstrated by some elaborately designed 3D ISE systems.

##### 4.1 Energy harvesting from air

The concept of exploiting energy input from the surrounding air was initially proposed as shown in Fig. 8(a)(i). This work [179] introduced the CESs (i.e., the evaporation surfaces without solar radiation) into a 3D ISE system (Fig. 8(a)(ii)). Due to the cooling effect of water evaporation, the CES temperature was lower than the ambient temperature, which led to the energy flow from the surrounding air to the evaporation system according to the

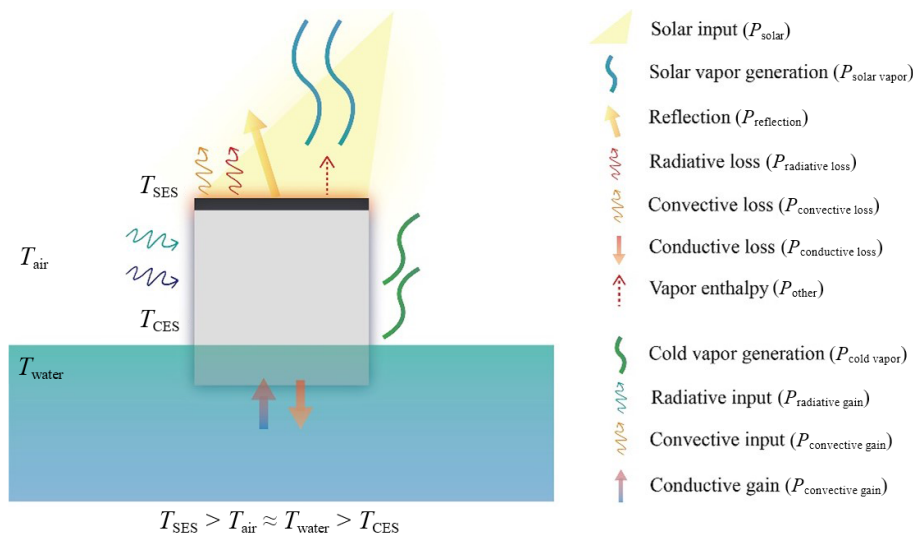


Figure 7 Schematic illustration of the energy nexus in typical 3D interfacial solar evaporation system.

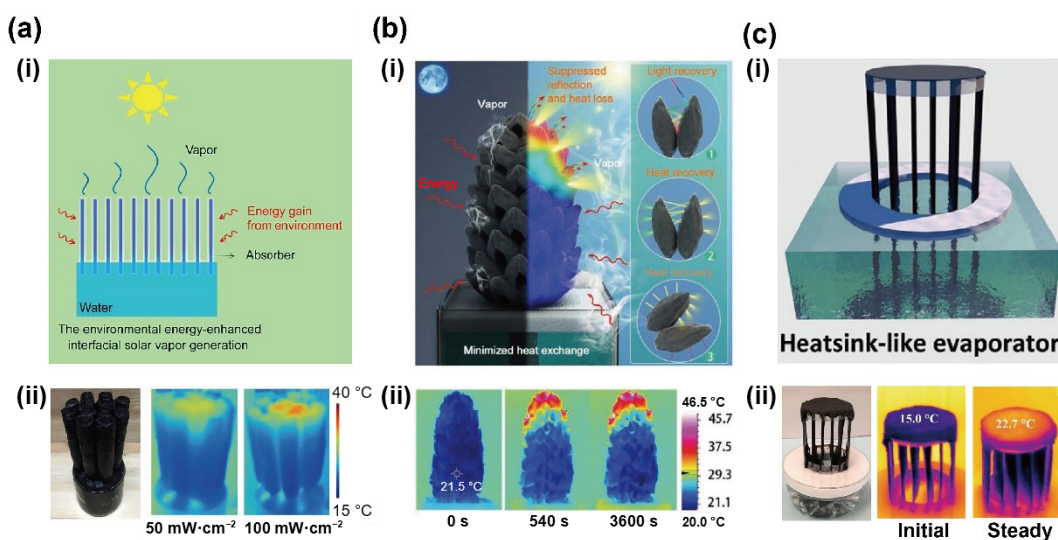


Figure 8 (a) Environmental energy-input assisted 3D interfacial solar evaporator composed of vertical cylindrical units: (i) schematic diagram of the environmental energy-enhanced interfacial solar vapor generator and (ii) photograph and IR images of the 3D interfacial solar evaporator composed of vertical cylindrical units. Reproduced with permission from Ref. [179], © Elsevier Inc. 2018. (b) Bio-based carbonized 3D pine tower evaporator with energy harvesting from surrounding air: (i) schematic diagram of the energy management of the carbonized 3D pine tower evaporator during solar evaporation and (ii) IR images of the carbonized 3D pine tower evaporator during solar evaporation. Reproduced with permission from Ref. [201], © Bian, Y. et al. 2019. (c) Heatsink-like interfacial solar evaporator with energy harvesting from the air: (i) diagram of the heatsink-like interfacial solar evaporator and (ii) IR images of the heatsink-like interfacial solar evaporator under 1 sun solar irradiation. Reproduced with permission from Ref. [202], © Wu, X. et al. 2021.

thermodynamics (Eqs. (4) and (5)). The environmental energy input as a complement of solar energy input contributed to the more efficient ISE process.

Inspired by the concept of environmental energy harvest, great advancements have been made towards highly efficient 3D ISE systems [66, 94, 100, 180–204]. The following designs that demonstrated excellent energy management reveal the significant progress in this field (Figs. 8(b) and 8(c)). Firstly, a bio-based pine tower design [201] realized a significant evaporation boost by enlarging spatial evaporation surfaces (Fig. 8(b)(i)). The dispersed branches on the 3D pine tower provided considerable CESs (Fig. 8(b)(ii)). In this regard, the more spatial evaporation surfaces, the more energy gained from the surrounding air, with a consequential increase in vapor generation on the surfaces. Theoretically, the spatial evaporation surfaces could be infinitely expanded by increasing in height or density. However, in practice, engineering issues, such as over-gravity water transportation,

mechanical support, and vapor escaping, also need to be considered in the system design. Therefore, a heat sink-like evaporator [202] was developed which maximized the passive thermal harvesting from the surroundings (Fig. 8(c)(i)). The principle of this design was to reverse the heat-sink cooling into thermally gaining energy from the environment. By optimizing the number of vertical slices, the evaporation performance could be enhanced. The energy utilization reached an outstanding level in the limited space. In addition, the cold fins successfully extracted energy from the above SES (i.e., solar evaporation surface), so that the temperature of SES was significantly decreased to be lower than the ambient environment (Fig. 8(c)(ii)). Therefore, all the evaporation surfaces of this 3D evaporator participated in cold evaporation under 1.0 sun irradiation which enabled a massive environmental energy to gain from all surfaces. The calculated energy gained from the surrounding environment is 170% of solar energy input.

## 4.2 Energy harvesting from bulk water

Recently, gaining energy from bulk water has been developed as a general and effective strategy for evaporation enhancement in 3D ISE systems [205–207]. Specifically, the presence of the CESs in 3D ISE systems forms the lower temperature zones compared to that of the ambient environment (i.e., air or water). The energy flows from the ambient environment to the CESs according to the thermodynamics. In this regard, extracting energy from water to the CESs has its theoretical basis which has led to the following research work [205]. With the optimization of 3D ISE designs, the energy flowing process was first revealed as shown in Fig. 9(a)(i). It started with the analysis of the temperature relationship between the objects in a 3D cylindrical ISE system, which noted as  $T_{\text{SES}} > T_{\text{water}} > T_{\text{CES}}$  (i.e., represented the temperature of the SES and bulk water and CES, respectively). The CES was considered as the end of energy flowing path in ISE process. Accordingly, the surface area for cold evaporation directly determined the capability of extracting energy from both energy sources of SES and water. If the CES area between the SES and bulk water was not sufficient, it cannot fully eliminate the conductive heat from the SES to the bulk water, which led to the net energy loss to the bulk water. While with the increase in CES area, the conductive heat flow

changed, as indicated in Fig. 9(a)(i). The sufficient area of CES enabled extraction of energy from bulk water in addition to the assimilation of the heat flow from SES, resulting in a net thermal energy flow from the bulk water to the evaporator. The direction of thermal energy flow was demonstrated by monitoring the temperature change of water held in a thermal insulator container with 3D ISE systems of different CES areas (Fig. 9(a)(ii)). In this 3D ISE system, when the height of evaporator reached 5 cm, the evaporator started to extract energy from the bulk water.

A very similar design [206] was reported to enhance solar evaporation by harvesting energy from bulk water (Fig. 9(b)). The 3D evaporator was directly obtained via an emulsion templating method. Engineering of the overall shape and internal pores produced a 3D evaporator that could suppress conduction heat loss and efficiently collect thermal energy from its surroundings, boosting the evaporation rate to  $2.82 \text{ kg}\cdot\text{m}^{-2}\cdot\text{h}^{-1}$  under 1.0 sun illumination. The structure of the evaporator is illustrated in Fig. 9(b)(i). The top solar absorbing layer connected to the side cold evaporation layer which was also the water transportation paths. The middle cavity was filled with air, designed for suppressing thermal energy loss from the top to the bottom. During solar evaporation, the temperature of CES kept lower than that of the

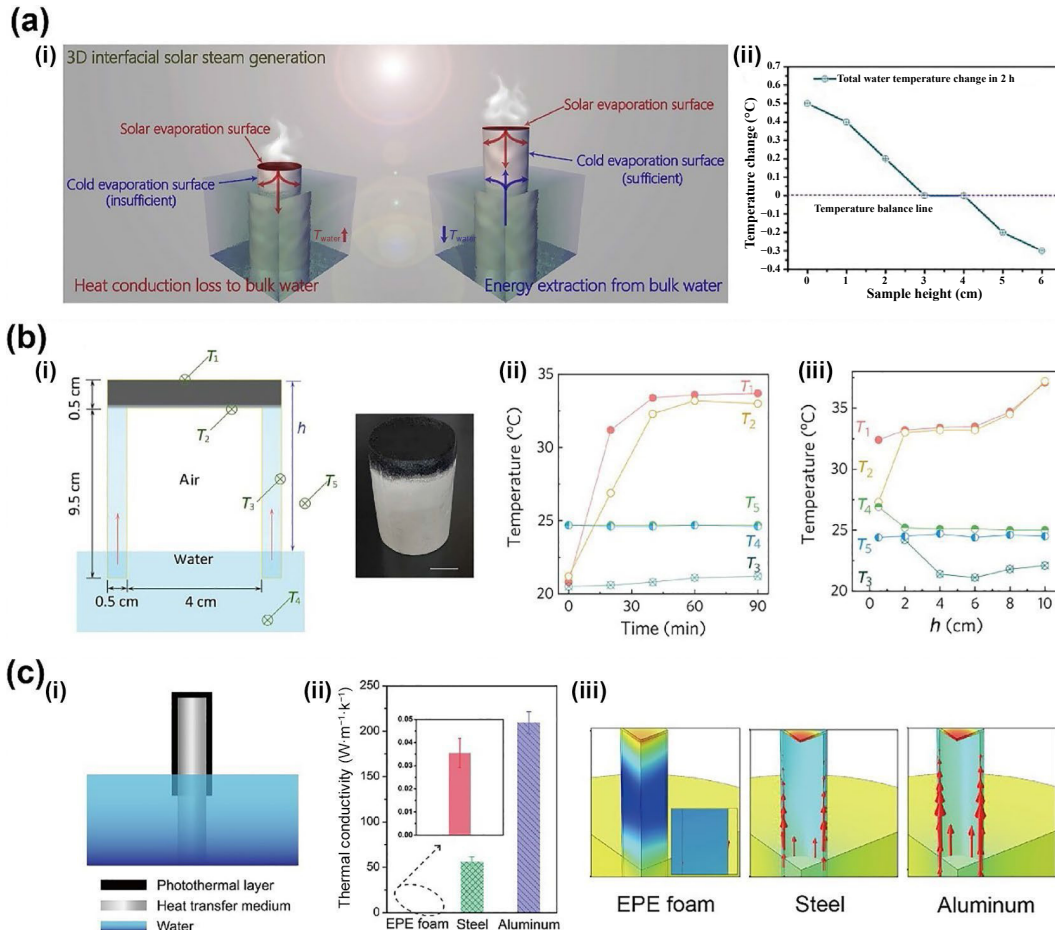


**Figure 9** (a) Concept of energy harvest from bulk water for evaporation boost in a 3D cylindrical ISE system: (i) schematic illustration of energy harvesting from bulk water in a 3D cylindrical ISE system and (ii) water temperature change in solar evaporation test with the increase in evaporator height. Reproduced with permission from Ref. [205], © Elsevier Ltd. 2020. (b) Water energy harvest in a 3D cylindrical ISE system: (i) structure diagram and photograph of the 3D cylindrical ISE evaporator, (ii) temperature change of the points in 3D cylindrical ISE system during solar evaporation, and (iii) temperature change of the points in solar evaporation test with the increase in evaporator height. Reproduced with permission from Ref. [206], © Chen, J. X. et al. 2022. (c) Rapid water energy extraction via highly thermally conductive evaporator support in a 3D cylindrical ISE system: (i) diagram of the 3D cylindrical ISE system with heat transfer medium as support, (ii) thermal conductivity of the supports, and (iii) numerical simulations of heat transfer process in 3D cylindrical ISE systems with different supports. Reproduced with permission from Ref. [207], © Science China Press 2021. Published by Elsevier B.V. and Science China Press.

solar absorber, air, and water (Fig. 9(b)(ii)). In terms of energy flow process, the bulk water temperature decreased, which confirmed the energy extraction from water to the evaporator. With the increase in the height of evaporator (i.e., increasing CES area), the water temperature was further reduced (Fig. 9(b)(ii)). It also demonstrated that more CES area promoted water energy extraction.

Although the thermal energy could be extracted from bulk water to evaporation surfaces for boosting water evaporation, it was not very efficient due to the low thermal conductivity of the used materials. Based on this, the rapid water energy extraction was studied by thermally connecting the CESs and the bulk water [207]. Instead of using typical thermal insulation materials, this 3D evaporator applied highly thermally conductive materials as evaporator support (Fig. 9(c)(i)). To demonstrate the relation between evaporation performance and thermal conductivity of the support, the expanded polystyrene foam (i.e., thermal insulation material), steel (i.e., thermally conductive material), and aluminum (i.e., highly thermally conductive) tubes were used as the support (Fig. 9(c)(ii)). The results showed with the increase in thermal conductivity of the evaporator support, the evaporation performance was significantly improved. Numerical simulations also proved that the highly thermally conductive path contributed to the much faster water energy extraction for evaporative utilization on CESs. This work also proved that the energy extracted from bulk water could be greater than the solar energy input. Therefore, energy harvesting from bulk water can be considered a practical strategy towards efficient solar evaporation in 3D ISE systems.

### 4.3 Advanced energy management via other strategies

Some recent work reported other strategies for boosting evaporation performance apart from obtaining energy from the environment. One representative approach was to complement solar evaporation enhancement by utilizing wind (i.e., air convective flow) [208–212]. The wind energy was regarded as a green and inexhaustible energy in nature. In practical water treatment, taking advantage of wind for solar evaporation could significantly enhance the evaporation rate because the wind could take away the generated vapor to maintain a low humidity environment near the evaporation surface for continuous evaporation. From the viewpoint of energy transfer, the evaporation surfaces were cooled down by the wind, which suppresses the energy loss via convection and radiation. If the wind is strong enough, the cooling effect could make the surface temperature lower than the environmental temperature, resulting in energy harvesting from the ambient environment during solar evaporation. Therefore, more energy is available to benefit efficient solar evaporation process. As shown in Fig. 10(a)(i), a porous 3D ISE evaporator [208] was introduced for boosting evaporation rate by wind. During solar evaporation, the convective flow crossed through the interconnected porous structure (Fig. 10(a)(ii)). The inner vapor was removed to the environment, which could activate the inner evaporation surfaces.

In addition, another kind of energy, the latent heat released from vapor condensation, was also collected and reused to increase water evaporation [213]. The released latent heat induced by vapor condensation normally exists above the solar evaporation surface due to the temperature difference between the air and the generated hot vapor. It was very hard to reabsorb the latent heat by a 2D flat evaporator (Fig. 10(b)(i)) because the latent heat was released into the air above the evaporation surface. While an

evaporator with vertical cold slices as CESs located above the SES enabled the absorption of the latent heat for evaporation enhancement in addition to the harvested energy from the surrounding air (Fig. 10(b)(ii)).

Very recently, an integrated evaporation design [214] was developed by combining solar electricity generation and solar evaporation, in which the solar cell was placed above the solar evaporator. Under solar radiation, the solar cell absorbed light photons above its bandgap, while the solar evaporator received the below-bandgap photons for thermal conversion. As depicted in Fig. 10(c)(i), the two modules in non-contact state led to low outputs in both parts due to the poor energy management in the integrated system. The solar cell had an issue that the generated heat decreased the solar-to-electricity efficiency. Meanwhile, the evaporation performance of the underneath evaporation surface was also inefficient because the solar light was partially absorbed by the solar cell above. To address the inappropriate thermal management of both solar cell and solar evaporator in the non-contact configuration, a thermally conductive bridge was introduced to connect the two parts (Fig. 10(c)(ii)). This modification successfully transferred the waste heat from solar cell to the evaporator. Therefore, the solar cell was cooled down which improved the efficiency of electricity generation. Concurrently, the evaporator received more heat which also improved the water evaporation rate.

### 4.4 Reduction of vaporization enthalpy by molecular engineering

So far, a feasible and promising approach to improve solar evaporation output from the same energy input is lowering water vaporization enthalpy by hierarchically structured hydrogels, for example, the hydrogels with 3D cross-linked polymer networks [122, 134, 142, 215–229]. The hydrophilicity of hydrogels is due to hydrophilic groups in polymer chains, including hydroxyl groups ( $-\text{OH}$ ), sulfonic acid groups ( $-\text{SO}_3\text{H}$ ), amino groups ( $-\text{NH}_2$ ), and carboxylic acid groups ( $-\text{COOH}$ ) (Fig. 11(a)(i)). These functional groups can bond with water molecules through noncovalent interactions such as hydrogen bonding and electrostatic interactions. Therefore, the state of the water in the hydrogel could be varied via adjusting functional groups of the hydrogel. In general, the water state in hydrogels is classified into three types, which are bound water, intermediate water, and free water (Fig. 11(a)(ii)). Free water is associated with water molecules whose structure is similar to that of bulk water, exhibiting negligible interaction with polymer chains. Bound water consists of water molecules that have strong interactions with functional groups in polymer chains. While intermediate water exists between free and bound water and interacts weakly with polymer chains, as well as adjacent water molecules. Therefore, the intermediate water has a reduced energy demand (i.e., evaporation enthalpy) for water evaporation, which is the core reason for boosting evaporation rate with same energy consumption. In addition to the proper functional group grafting, structures of polymer networks also determine the content of intermediate water in the hydrogels [230–232]. The nano-porous hydrogel enables the regulation of water state by hierarchical water pathways in the hydrogel (Figs. 11(b)(i) and 11(b)(ii)), including internal gaps, micron channels, and molecular meshes [218]. These structures also provide fast water pumping and diffusion to sustain high-rate water evaporation. The converted solar thermal energy can be efficiently utilized to power the vaporization of water contained in the

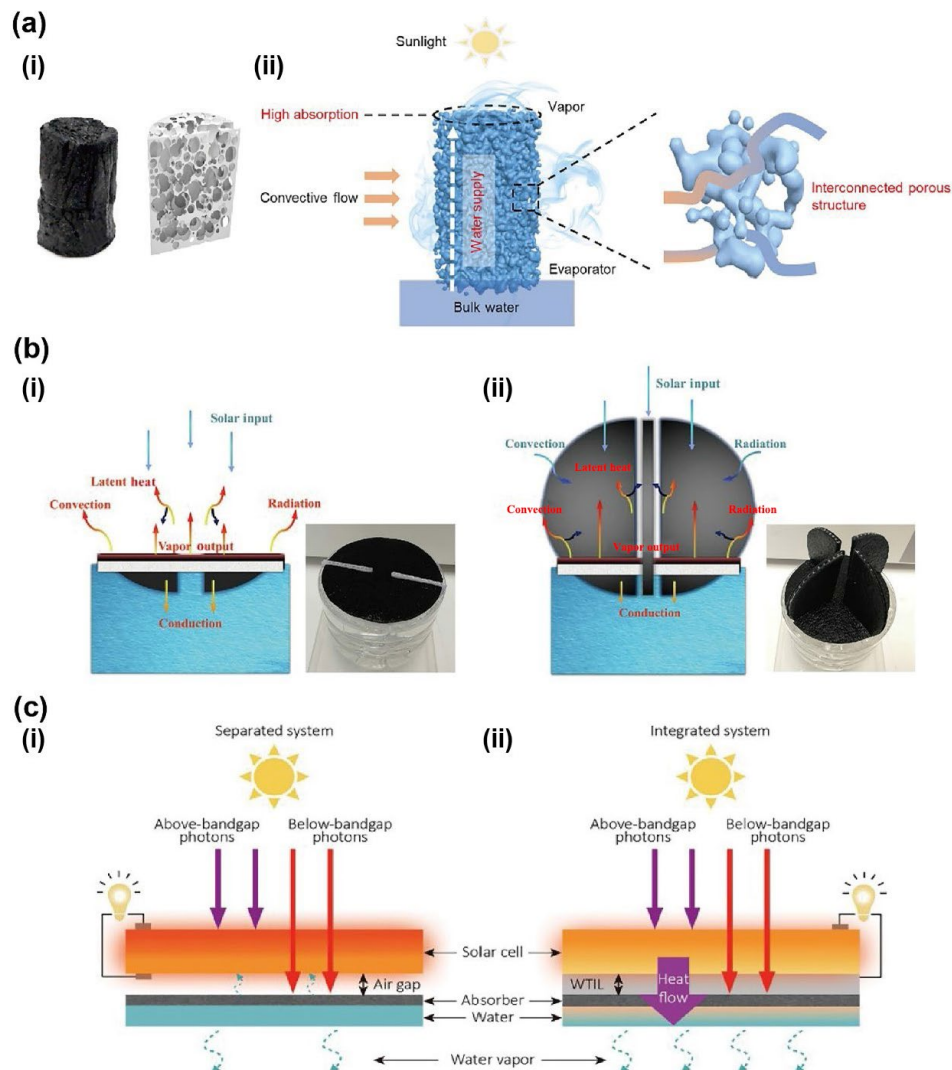


**Figure 10** (a) The concept of evaporation enhancement in a porous 3D ISE evaporator via convective flow: (i) photograph and structural diagram of 3D porous evaporator and (ii) schematic illustration of solar evaporation process over a 3D porous evaporator with assistance of convective flow. Reproduced with permission from Ref. [208], © Elsevier Inc. 2020. (b) The concept of boosting evaporation by recycling latent heat: (i) left: the energy flux of a typical 2D evaporator during solar evaporation and right: the photograph of the typical 2D evaporator. (ii) Left: the energy flux of a fin-structured 3D evaporator during solar evaporation and right: the photograph of the fin-structure 3D evaporator. Reproduced with permission from Ref. [213], © Science China Press 2020. Published by Elsevier B.V. and Science China Press. (c) The concept of applying conductive energy from solar cell for interfacial solar evaporation enhancement: (i) the energy flux diagram of the solar cell integrated evaporator with an air gap between them and (ii) the energy flux diagram of the solar cell integrated evaporator with full contact between them. Reproduced with permission from Ref. [214], © Elsevier Inc. 2019.

molecular meshes of the poly(vinyl alcohol) (PVA) network, where the skeleton of the hydrogel facilitates water evaporation. With the decreased vaporization enthalpy and hierarchically structure construction, the evaporation rate can be greatly boosted which is now an extensively applied strategy for highly efficient ISE.

Inspired by this concept, some work reported very high evaporation rates achieved by optimized designs of hydrogels [87, 110, 233–236]. For example, a hierarchical structure was constructed using 2D materials (MXene and reduced graphene oxide) and 3D networks (PVA and chitosan) [87], as depicted in Fig. 11(c). With rich functional groups and elaborated porous structure, the hydrogel significantly reduced the water vaporization enthalpy and improved water transportation by the 3D network, leading to remarkable evaporation rate enhancement. Another hydrogel (Fig. 11(d)) [236] with integrated hybrid regions of covalent organic framework (COF) and graphene realized a very high water evaporation rate of  $3.69 \text{ kg}\cdot\text{m}^{-2}\cdot\text{h}^{-1}$  under 1 sun

irradiation. Apart from the micro- and nanoscale controlling of structure and functional group, regional regulation of hydrophilicity by adjusting the content of the covalent organic framework and graphene in hydrogel is also accountable for evaporation rate enhancement. This strategy well optimized the water content and state in the hydrogel, resulting in significant reduction in water vaporization enthalpy. Additionally, the elaborated 3D porous hydrogels could also sustain high evaporation rate in practical brine treatment [237, 238]. Compared with most evaporators without structural design, the hierarchically structured hydrogels induce accelerated water flow by the abundant channels, which offers a potential approach to avoid salt fouling on evaporation surfaces and continuously evaporate water at high rate during practical desalination process.

## 5 Conclusion and perspectives

Based on the in-depth understanding of the energy nexus in

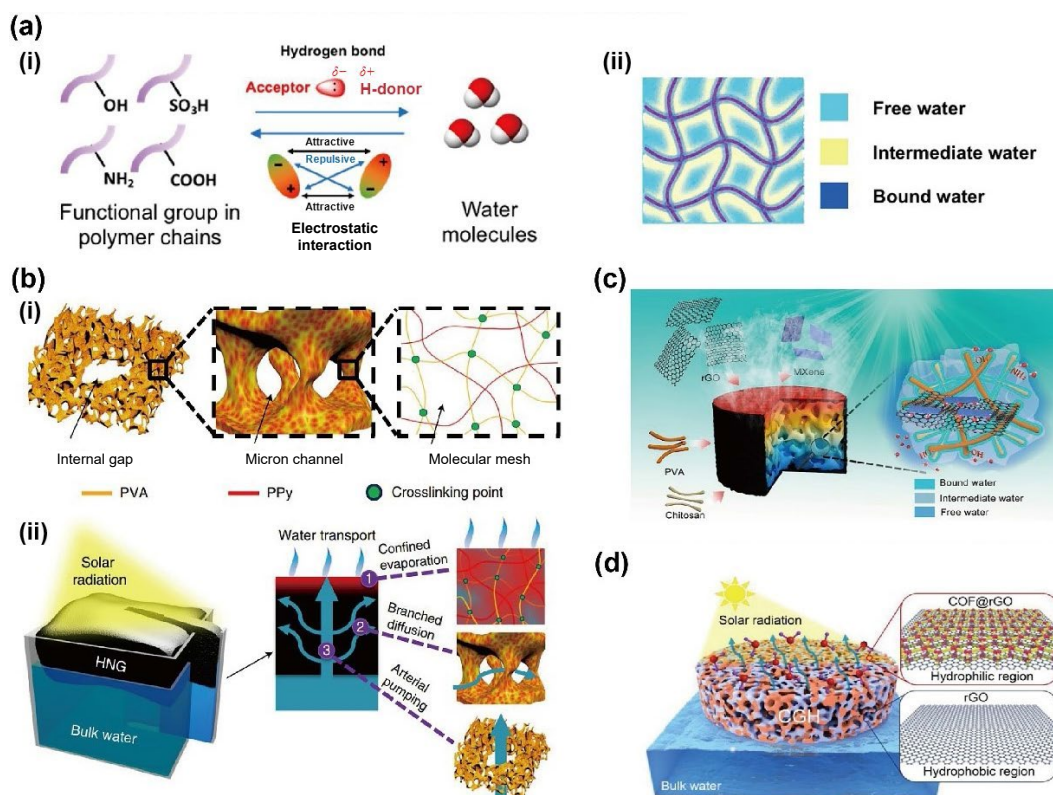


**Figure 11** (a) Diagram of bonding effect between functional groups and water molecules: (i) noncovalent interactions between water molecules and functional groups in polymer chains and (ii) unique water state in hydrogels. Reproduced with permission from Ref. [216], © American Chemical Society 2019. (b) Schematic illustration of highly efficient solar vapour generation based on tailored water transportation in hierarchically structured hydrogel: (i) The hydrogel consists of hierarchical porous structures, including internal gaps, micron channels, and molecular meshes. (ii) Schematic illustration of a typical solar vapour generation system and the water confinement strategy. Reproduced with permission from Ref. [218], © Macmillan Publishers Limited, part of Springer Nature 2018. (c) Schematic illustration of the vaporization enthalpy reduction caused by the synergy of tailored water states in confined space and concave pyramid-shaped surface topography of MXene/rGO-embedded hybrid hydrogels. Reproduced with permission from Ref. [87], © American Chemical Society 2021. (d) Scheme of the COF/graphene dual-region hydrogel for accelerating solar-driven water evaporation. Reproduced with permission from Ref. [236], © American Chemical Society 2022.

interfacial solar evaporation systems, the main principles for achieving highly efficient solar evaporation are as follows: (1) avoiding energy loss from the evaporation systems to the environment; (2) expanding energy input from the surrounding air and bulk water; (3) making full use of the existing energy already in the evaporation systems; (4) lowering the evaporation enthalpy. In addition, it should point out that due to the significantly different energy nexus in 2D and 3D ISE systems, the principles for designing evaporators are also different, especially for heat energy exchange between evaporators and bulk water. For a 2D ISE system, heat conduction loss from evaporation surface to bulk water is inevitable, thus thermal insulating evaporator support is necessary. While for 3D ISE system, it is possible to extract energy from bulk water to the evaporator, thus highly thermally conductive support is favourable. In recent years, numerous studies have proven the feasibility of these strategies through optimizing materials, structures, configurations, and processes of ISE systems. Highly efficient ISE systems thus have been designed and fabricated. However, there are still many opportunities to further improve evaporation performance towards practical applications, especially on a 3D spatial scale, for example, introducing new energy sources for evaporation, exploring more cost-effective photothermal materials and innovative evaporators, improving vapor condensation and collection efficiency, increasing clean water production within a limited space, and developing large-scale interfacial solar evaporation systems toward practical applications.

In the current context of worldwide clean water shortages and advocacy for low carbon emission technologies, ISE is now accepted as one of the most promising technologies to solve the global clean water scarcity issues. However, there is still a long way to go to push forward the real-world applications of ISE technology. The following aspects need to be considered for constructing next-generation ISE systems towards practical applications:

(1) The first notable aspect is introducing new energy sources for ISE. Solar light intensity significantly varies with weather conditions, on rainy, cloudy days, and at night, the energy input from sunlight dramatically decreases, resulting in a significant decrease in clean water production. In this regard, exploring new energy sources is of importance in the development of all-day, all-weather, and all-season interfacial solar evaporation systems. Other than extra energy harvest from the surrounding air and bulk water, Joule heating as an active heating approach could be considered for energy supply in situations where clean water is urgently needed but sunlight is not available. In addition, using phase change materials to store the surplus thermal energy during the daytime and release it at night is also a potential way to produce a considerable amount of water without light.

(2) The second aspect of developing next-generation ISE systems is to continuously explore novel photothermal materials. Materials with excellent solar-to-thermal energy conversion and low emissivity are the basic consideration for constructing solar evaporators. The next-stage development of photothermal

materials needs to focus on maximizing the utilization of thermal energy in both macroscale and micro-nanoscale. The thermal conductivity of photothermal materials also needs to be regulated to optimize the thermal energy distribution and utilization based on the structure of the evaporator (2D or 3D). In addition, reducing material costs is also essential for application-oriented consideration. Although ISE is an environmentally friendly technology for freshwater production, it needs to be more cost-effective to compensate for its low clean water production relative to osmosis desalination. Developing strategies for more vapor output using less material is highly favourable [151].

(3) Exploration of innovative designs of photothermal evaporators will be an important aspect of future work. Thermal energy management, water flow regulation, and salt resistance are all related to the evaporator design. A desired evaporator should be able to integrate multiple functions in one unit. For example, it needs to maximize energy harvest and utilization for water evaporation, while optimizing the water flow to ensure balanced water supply and evaporation, as well as avoiding salt accumulation on evaporation surfaces.

(4) Improving water production in a limited space is another important research direction. In an ISE system, water evaporation and collection are two main parts. Rapid water evaporation is the prerequisite for fast water collection, but it does not mean rapid water collection. Although very high solar evaporation rates have been achieved, highly efficient water collection is rarely reported. The water collection rate determines the actual clean water production in interfacial solar evaporation systems. The desired ISE system should contain an excellent water evaporation module and an efficient vapor condensing module in a compact space, so that it has real potential for real-world application.

(5) Developing large-scale interfacial solar evaporation systems is of great significance for practical applications, especially for seawater desalination and wastewater treatment. However, system scaling-up is not to directly apply larger evaporation surfaces, since it has been demonstrated that with the increase of the size of the evaporation surface, the evaporation rate decreases. Therefore, a better choice for constructing large-scale interfacial solar evaporation systems is to produce small evaporators as units and assemble them in appropriate patterns to form an interconnected system.

## Acknowledgements

Authors acknowledge the support of the National Natural Science Foundation of China (Nos. 52125201 and 21975141), the National Key Basic Research and Development Program (No. 2020YFA0210702), Shenzhen Science and Technology Research Project (No. JCYJ20180508152903208), and Australian Research Council (Nos. FT190100485 and DP220100583).

## Declaration of conflicting interests

The authors declare no conflicting interests regarding the content of this article.

## References

- Salehi, M. Global water shortage and potable water safety; today's concern and tomorrow's crisis. *Environ. Int.* **2022**, *158*, 106936.
- Mishra, B. K.; Kumar, P.; Saraswat, C.; Chakraborty, S.; Gautam, A. Water security in a changing environment: Concept, challenges and solutions. *Water* **2021**, *13*, 490.
- Boretti, A.; Rosa, L. Reassessing the projections of the World Water Development Report. *npj Clean Water* **2019**, *2*, 15.
- Wu, J. Y. Challenges for safe and healthy drinking water in China. *Curr. Environ. Health Rep.* **2020**, *7*, 292–302.
- McDonald, R. I.; Green, P.; Balk, D.; Fekete, B. M.; Revenga, C.; Todd, M.; Montgomery, M. Urban growth, climate change, and freshwater availability. *Proc. Natl. Acad. Sci. USA* **2011**, *108*, 6312–6317.
- Kummu, M.; Ward, P. J.; de Moel, H.; Varis, O. Is physical water scarcity a new phenomenon? Global assessment of water shortage over the last two millennia. *Environ. Res. Lett.* **2010**, *5*, 034006.
- Curto, D.; Franzitta, V.; Guercio, A. A review of the water desalination technologies. *Appl. Sci.* **2021**, *11*, 670.
- Darre, N. C.; Toor, G. S. Desalination of water: A review. *Curr. Pollut. Rep.* **2018**, *4*, 104–111.
- Nassrullah, H.; Anis, S. F.; Hashaikeh, R.; Hilal, N. Energy for desalination: A state-of-the-art review. *Desalination* **2020**, *491*, 114569.
- Gebreyesus, G. D. Status of hybrid membrane-ion-exchange systems for desalination: A comprehensive review. *Appl. Water Sci.* **2019**, *9*, 135.
- Adham, S.; Hussain, A.; Matar, J. M.; Dores, R.; Janson, A. Application of membrane distillation for desalting brines from thermal desalination plants. *Desalination* **2013**, *314*, 101–108.
- Shaulsky, E.; Wang, Z. X.; Deshmukh, A.; Karanikola, V.; Elimelech, M. Membrane distillation assisted by heat pump for improved desalination energy efficiency. *Desalination* **2020**, *496*, 114694.
- Goosen, M. F. A.; Sablani, S. S.; Al-Hinai, H.; Al-Obeidani, S.; Al-Belushi, R.; Jackson, D. Fouling of reverse osmosis and ultrafiltration membranes: A critical review. *Sep. Sci. Technol.* **2005**, *39*, 2261–2297.
- Politano, A.; Argurio, P.; Di Profio, G.; Sanna, V.; Cupolillo, A.; Chakraborty, S.; Arafat, H. A.; Curcio, E. Photothermal membrane distillation for seawater desalination. *Adv. Mater.* **2017**, *29*, 1603504.
- Wang, Z. X.; Horseman, T.; Straub, A. P.; Yip, N. Y.; Li, D. Y.; Elimelech, M.; Lin, S. H. Pathways and challenges for efficient solar-thermal desalination. *Sci. Adv.* **2019**, *5*, eaax0763.
- Zhu, L. L.; Gao, M. M.; Peh, C. K. N.; Ho, G. W. Recent progress in solar-driven interfacial water evaporation: Advanced designs and applications. *Nano Energy* **2019**, *57*, 507–518.
- Gao, M. M.; Peh, C. K.; Meng, F. L.; Ho, G. W. Photothermal membrane distillation toward solar water production. *Small Methods* **2021**, *5*, 2001200.
- He, F.; Wu, X. C.; Gao, J.; Wang, Z. X. Solar-driven interfacial evaporation toward clean water production: Burgeoning materials, concepts and technologies. *J. Mater. Chem. A* **2021**, *9*, 27121–27139.
- Wu, X.; Chen, G. Y.; Owens, G.; Chu, D. W.; Xu, H. L. Photothermal materials: A key platform enabling highly efficient water evaporation driven by solar energy. *Mater. Today Energy* **2019**, *12*, 277–296.
- Cao, S. S.; Rathi, P.; Wu, X. H.; Ghim, D.; Jun, Y. S.; Singamaneni, S. Cellulose nanomaterials in interfacial evaporators for desalination: A “natural” choice. *Adv. Mater.* **2021**, *33*, 2000922.
- Ding, T. P.; Zhou, Y.; Ong, W. L.; Ho, G. W. Hybrid solar-driven interfacial evaporation systems: Beyond water production towards high solar energy utilization. *Mater. Today* **2021**, *42*, 178–191.
- Poletti, A.; Fracasso, G.; Conti, G.; Pilot, R.; Amendola, V. Laser generated gold nanocorals with broadband plasmon absorption for photothermal applications. *Nanoscale* **2015**, *7*, 13702–13714.
- Cheng, P. F.; Wang, D.; Schaaf, P. A review on photothermal conversion of solar energy with nanomaterials and nanostructures: From fundamentals to applications. *Adv. Sustain. Syst.* **2022**, *6*, 2200115.
- Huang, X.; Liu, J. Z.; Zhou, P.; Su, G. H.; Zhou, T.; Zhang, X. X.;

- Zhang, C. H. Ultrarobust photothermal materials via dynamic crosslinking for solar harvesting. *Small* **2022**, *18*, 2104048.
- [25] Chen, W.; Miao, H.; Meng, G. Q.; Huang, K. L.; Kong, L. Q.; Lin, Z. F.; Wang, X. D.; Li, X. B.; Li, J. H.; Liu, X. Y. et al. Polydopamine-induced multilevel engineering of regenerated silk fibroin fiber for photothermal conversion. *Small* **2022**, *18*, 2107196.
- [26] Shridharan, T. S.; Kang, M. J.; Sivanantham, A.; Kim, S.; Cho, I. S. Layered bismuth copper oxychalcogenides as advanced photothermal materials for efficient interfacial solar desalination. *Desalination* **2022**, *540*, 115984.
- [27] Xiao, P.; Yang, W. Q.; Qiu, N. X.; Li, S.; Ni, F.; Zhang, C.; Gu, J. C.; Kuo, S. W.; Chen, T. Engineering biomimetic nanostructured “melanosome” textiles for advanced solar-to-thermal devices. *Nano Lett.* **2022**, *22*, 9343–9350.
- [28] Cao, S. J.; Thomas, A.; Li, C. X. Emerging materials for interfacial solar-driven water purification. *Angew. Chem., Int. Ed.* **2023**, *62*, e202214391.
- [29] Hao, S. Y.; Han, H. C.; Yang, Z. Y.; Chen, M. T.; Jiang, Y. Y.; Lu, G. X.; Dong, L.; Wen, H. L.; Li, H.; Liu, J. R. et al. Recent advancements on photothermal conversion and antibacterial applications over MXenes-based materials. *Nano-Micro Lett.* **2022**, *14*, 178.
- [30] Huang, Z. M.; Liu, Y.; Li, S. L.; Lee, C. S.; Zhang, X. H. From materials to devices: Rationally designing solar steam system for advanced applications. *Small Methods* **2022**, *6*, 2200835.
- [31] Zang, L. L.; Finnerty, C.; Zheng, S. X.; Conway, K.; Sun, L. G.; Ma, J.; Mi, B. X. Interfacial solar vapor generation for desalination and brine treatment: Evaluating current strategies of solving scaling. *Water Res.* **2021**, *198*, 117135.
- [32] Li, J. Y.; Jing, Y. J.; Zhou, X.; Mao, J. L.; Chen, Y. J.; Sun, H. X.; Deng, X. F.; Gao, C. Z. Multifunctional photothermal materials based on natural pumices for high efficiency solar-driven interface evaporator. *Int. J. Energy Res.* **2021**, *45*, 20132–20142.
- [33] Ibrahim, I.; Bhoopal, V.; Seo, D. H.; Afsari, M.; Shon, H. K.; Tijjng, L. D. Biomass-based photothermal materials for interfacial solar steam generation: A review. *Mater. Today Energy* **2021**, *21*, 100716.
- [34] Xie, Z. J.; Duo, Y. H.; Lin, Z. T.; Fan, T. J.; Xing, C. Y.; Yu, L.; Wang, R. H.; Qiu, M.; Zhang, Y. P.; Zhao, Y. H. et al. The rise of 2D photothermal materials beyond graphene for clean water production. *Adv. Sci.* **2020**, *7*, 1902236.
- [35] Lin, Y. W.; Xu, H.; Shan, X. L.; Di, Y. S.; Zhao, A. Q.; Hu, Y. J.; Gan, Z. X. Solar steam generation based on the photothermal effect: From designs to applications, and beyond. *J. Mater. Chem. A* **2019**, *7*, 19203–19227.
- [36] Zhang, Y.; Wang, Y.; Yu, B.; Yin, K. B.; Zhang, Z. H. Hierarchically structured black gold film with ultrahigh porosity for solar steam generation. *Adv. Mater.* **2022**, *34*, 2200108.
- [37] Wang, Z. X.; Gao, J.; Zhou, J. J.; Gong, J. W.; Shang, L. W.; Ye, H. B.; He, F.; Peng, S. Q.; Lin, Z. X.; Li, Y. X. et al. Engineering metal-phenolic networks for solar desalination with directional salt crystallization. *Adv. Mater.* **2023**, *35*, 2209015.
- [38] Kiriarachchi, H. D.; Awad, F. S.; Hassan, A. A.; Bobb, J. A.; Lin, A.; El-Shall, M. S. Plasmonic chemically modified cotton nanocomposite fibers for efficient solar water desalination and wastewater treatment. *Nanoscale* **2018**, *10*, 18531–18539.
- [39] Zhang, L. L.; Xing, J.; Wen, X. L.; Chai, J. W.; Wang, S. J.; Xiong, Q. H. Plasmonic heating from indium nanoparticles on a floating microporous membrane for enhanced solar seawater desalination. *Nanoscale* **2017**, *9*, 12843–12849.
- [40] Wang, Z. H.; Liu, Y. M.; Tao, P.; Shen, Q. C.; Yi, N.; Zhang, F. Y.; Liu, Q. L.; Song, C. Y.; Zhang, D.; Shang, W. et al. Bio-inspired evaporation through plasmonic film of nanoparticles at the air–water interface. *Small* **2014**, *10*, 3234–3239.
- [41] Wu, T.; Li, H. X.; Xie, M. H.; Shen, S.; Wang, W. X.; Zhao, M.; Mo, X. M.; Xia, Y. N. Incorporation of gold nanocages into electrospun nanofibers for efficient water evaporation through photothermal heating. *Mater. Today Energy* **2019**, *12*, 129–135.
- [42] Zhang, M.; Xu, W. H.; Li, M. F.; Li, J. Q.; Wang, P.; Wang, Z. K. *In situ* reduction of silver nanoparticles on chitosan hybrid copper phosphate nanoflowers for highly efficient plasmonic solar-driven interfacial water evaporation. *J. Bionic. Eng.* **2021**, *18*, 30–39.
- [43] Yang, Y. W.; Que, W. X.; Zhao, J. Q.; Han, Y.; Ju, M. M.; Yin, X. T. Membrane assembled from anti-fouling copper-zinc-tin-selenide nanocarambolas for solar-driven interfacial water evaporation. *Chem. Eng. J.* **2019**, *373*, 955–962.
- [44] Li, N.; Yin, D. D.; Xu, L. L.; Zhao, H. Y.; Liu, Z. Q.; Du, Y. P. High-quality ultralong copper sulphide nanowires for promising applications in high efficiency solar water evaporation. *Mater. Chem. Front.* **2019**, *3*, 394–398.
- [45] Shao, B.; Wang, Y. D.; Wu, X.; Lu, Y.; Yang, X. F.; Chen, G. Y.; Owens, G.; Xu, H. L. Stackable nickel-cobalt@polydopamine nanosheet based photothermal sponges for highly efficient solar steam generation. *J. Mater. Chem. A* **2020**, *8*, 11665–11673.
- [46] Zhou, L.; Tan, Y. L.; Wang, J. Y.; Xu, W. C.; Yuan, Y.; Cai, W. S.; Zhu, S. N.; Zhu, J. 3D self-assembly of aluminium nanoparticles for plasmon-enhanced solar desalination. *Nat. Photonics* **2016**, *10*, 393–398.
- [47] Zakaria, H.; Li, Y.; Fathy, M. M.; Zhou, X. Y.; Xiong, X. Y.; Wang, Y.; Rong, S. X.; Zhang, C. A novel TiO<sub>(2-x)</sub>/TiN@ACB composite for synchronous photocatalytic Cr(VI) reduction and water photothermal evaporation under visible/infrared light illumination. *Chemosphere* **2022**, *311*, 137137.
- [48] Ying, P. J.; Li, M.; Yu, F. L.; Geng, Y.; Zhang, L. Y.; He, J. J.; Zheng, Y. J.; Chen, R. Band gap engineering in an efficient solar-driven interfacial evaporation system. *ACS Appl. Mater. Interfaces* **2020**, *12*, 32880–32887.
- [49] Yang, M. Q.; Tan, C. F.; Lu, W. H.; Zeng, K. Y.; Ho, G. W. Spectrum tailored defective 2D semiconductor nanosheets aerogel for full-spectrum-driven photothermal water evaporation and photochemical degradation. *Adv. Funct. Mater.* **2020**, *30*, 2004460.
- [50] Zhu, S. H.; Lei, Z. W.; Dou, Y. J.; Lou, C. W.; Lin, J. H.; Li, J. W. Sputter-deposited nickel nanoparticles on Kevlar fabrics with laser-induced graphene for efficient solar evaporation. *Chem. Eng. J.* **2023**, *452*, 139403.
- [51] Zheng, P.; Tang, J. L.; Zhou, Z. P.; Gong, L.; Yang, H. F.; Jia, X.; Li, X. D.; Liu, Y. S.; Tan, L. H. Ultrafast synthesis of defective black TiO<sub>2</sub> via one-step NaN<sub>3</sub> deflagration for high-efficiency solar water evaporation. *Surf. Interfaces* **2021**, *22*, 100901.
- [52] Wei, N.; Li, Z. K.; Li, Q.; Yang, E. Q.; Xu, R. Q.; Song, X. J.; Sun, J. Q.; Dou, C.; Tian, J.; Cui, H. Z. Scalable and low-cost fabrication of hydrophobic PVDF/WS<sub>2</sub> porous membrane for highly efficient solar steam generation. *J. Colloid Interface Sci.* **2021**, *588*, 369–377.
- [53] Wang, Y. Z.; Zhao, L.; Zhang, F.; Yu, K.; Yang, C. Y.; Jia, J. J.; Guo, W.; Zhao, J. X.; Qu, F. Y. Synthesis of a Co-Sn alloy-deposited PTFE film for enhanced solar-driven water evaporation via a super-absorbent polymer-based “water pump” design. *ACS Appl. Mater. Interfaces* **2021**, *13*, 26879–26890.
- [54] Wang, L. F.; Yang, G. L.; Jiang, L.; Ma, Y. X.; Liu, D.; Raza, J.; Lei, W. W. Improved photo-excited carriers transportation of WS<sub>2</sub>-O-doped-graphene heterostructures for solar steam generation. *Small* **2022**, 2204898.
- [55] Si, P. C.; Wang, Q. H.; Kong, H. R.; Li, Y. T.; Wang, Y. Gradient titanium oxide nanowire film: A multifunctional solar energy utilization platform for high-salinity organic sewage treatment. *ACS Appl. Mater. Interfaces* **2022**, *14*, 19652–19658.
- [56] Qiu, X. P.; Kong, H. R.; Li, Y. T.; Wang, Q. H.; Wang, Y. Interface engineering of a Ti<sub>4</sub>O<sub>7</sub> nanofibrous membrane for efficient solar-driven evaporation. *ACS Appl. Mater. Interfaces* **2022**, *14*, 54855–54866.
- [57] Miao, X.; Zhao, L.; Ren, G. N.; Pang, Y. L.; Xin, H.; Ge, B.; Liu, C. C. Design of an interface heating device based on polydivinylbenzene/SiO<sub>2</sub>/Bi<sub>2</sub>WO<sub>6</sub> and its visible light response

- performance for water purification. *Phys. Chem. Chem. Phys.* **2023**, *25*, 4332–4339.
- [58] Liu, W. N.; Li, P. F.; Li, X. Q.; He, Y. Q.; An, L.; Qu, D.; Wang, X. Y.; Sun, Z. C. Self-cleaning solar water evaporation device based on polyaniline/TiO<sub>2</sub>/natural cellulose fibers for contaminant water. *Sci. China Mater.*, in press, <https://doi.org/10.1007/s40843-022-2282-9>.
- [59] Li, W.; Li, X. F.; Liu, J.; Zeng, M. J.; Feng, X. Y.; Jia, X. Q.; Yu, Z. Z. Coating of wood with Fe<sub>2</sub>O<sub>3</sub>-decorated carbon nanotubes by one-step combustion for efficient solar steam generation. *ACS Appl. Mater. Interfaces* **2021**, *13*, 22845–22854.
- [60] Li, D.; Chen, S. S.; Huang, R. R.; Xue, C. R.; Li, P. F.; Li, Y. S.; Chang, Q.; Wang, H. Q.; Li, N.; Jia, S. P. et al. Photothermal, photocatalytic, and anti-bacterial Ti-Ag-O nanoporous powders for interfacial solar driven water evaporation. *Ceram. Int.* **2021**, *47*, 19800–19808.
- [61] Han, S.; Yang, J.; Li, X. F.; Li, W.; Zhang, X. T.; Koratkar, N.; Yu, Z. Z. Flame synthesis of superhydrophilic carbon nanotubes/Ni foam decorated with Fe<sub>2</sub>O<sub>3</sub> nanoparticles for water purification via solar steam generation. *ACS Appl. Mater. Interfaces* **2020**, *12*, 13229–13238.
- [62] Du, R. R.; Zhu, H. Y.; Zhao, H. Y.; Lu, H.; Dong, C.; Liu, M. T.; Yang, F.; Yang, J.; Wang, J.; Pan, J. M. Coupling ultrafine plasmonic Co<sub>3</sub>O<sub>4</sub> with thin-layer carbon over SiO<sub>2</sub> nanosphere for dual-functional PMS activation and solar interfacial water evaporation. *J. Alloys Compd.* **2023**, *940*, 168816.
- [63] Ai, L. H.; Xu, Y.; Qin, S.; Luo, Y.; Wei, W.; Wang, X. Z.; Jiang, J. Facile fabrication of Ni<sub>5</sub>P<sub>4</sub>-NiMoO<sub>4</sub> nanorod arrays with synergistic thermal management for efficient interfacial solar steam generation and water purification. *J. Colloid Interface Sci.* **2023**, *634*, 22–31.
- [64] Ahmad Wani, T.; Garg, P.; Bera, S.; Bhattacharya, S.; Dutta, S.; Kumar, H.; Bera, A. Narrow-bandgap LaMO<sub>3</sub> (M = Ni, Co) nanomaterials for efficient interfacial solar steam generation. *J. Colloid Interface Sci.* **2022**, *612*, 203–212.
- [65] Zhang, L.; Liu, G.; Wu, L. P.; Chen, Z. H.; Dai, Z. Y.; Yu, F.; Wang, X. B. Integrated light adsorption and thermal insulation of Zn doping 1T phase MoS<sub>2</sub>-based evaporation prototype for continuous freshwater generation. *Chem. Eng. J.* **2023**, *454*, 140298.
- [66] Yang, E. Q.; Wei, N.; Li, M. H.; Xu, R. Q.; Sui, Y. L.; Kong, M. Y.; Ran, X. C.; Cui, H. Z. Three-dimensional artificial transpiration structure based on 1T/2H-MoS<sub>2</sub>/activated carbon fiber cloth for solar steam generation. *ACS Appl. Mater. Interfaces* **2022**, *14*, 29788–29796.
- [67] Wu, J.; Qu, J.; Yin, G.; Zhang, T. T.; Zhao, H. Y.; Jiao, F. Z.; Liu, J.; Li, X. F.; Yu, Z. Z. Omnidirectionally irradiated three-dimensional molybdenum disulfide decorated hydrothermal pinecone evaporator for solar-thermal evaporation and photocatalytic degradation of wastewaters. *J. Colloid Interface Sci.* **2023**, *637*, 477–488.
- [68] Liu, P.; Hu, Y. B.; Li, X. Y.; Xu, L.; Chen, C.; Yuan, B. L.; Fu, M. L. Enhanced solar evaporation using a scalable MoS<sub>2</sub>-based hydrogel for highly efficient solar desalination. *Angew. Chem., Int. Ed.* **2022**, *61*, e202208587.
- [69] Lin, Z. X.; Wu, T. T.; Feng, Y. F.; Shi, J.; Zhou, B.; Zhu, C. H.; Wang, Y. Y.; Liang, R. L.; Mizuno, M. Poly(N-phenylglycine)/MoS<sub>2</sub> nanohybrid with synergistic solar-thermal conversion for efficient water purification and thermoelectric power generation. *ACS Appl. Mater. Interfaces* **2022**, *14*, 1034–1044.
- [70] Li, M.; Liu, B. W.; Guo, H. M.; Wang, H. T.; Shi, Q. Y.; Xu, M. W.; Yang, M. Q.; Luo, X. B.; Wang, L. D. Reclaimable MoS<sub>2</sub> sponge absorbent for drinking water purification driven by solar energy. *Environ. Sci. Technol.* **2022**, *56*, 11718–11728.
- [71] Guo, M. Y.; Yuan, B. H.; Sui, Y.; Xiao, Y.; Dong, J.; Yang, L. X.; Bai, L. J.; Yang, H. W.; Wei, D. L.; Wang, W. X. et al. Rational design of molybdenum sulfide/tungsten oxide solar absorber with enhanced photocatalytic degradation toward dye wastewater purification. *J. Colloid Interface Sci.* **2023**, *631*, 33–43.
- [72] Chen, R.; Wang, X.; Gan, Q. M.; Zhang, T. Q.; Zhu, K. H.; Ye, M. M. A bifunctional MoS<sub>2</sub>-based solar evaporator for both efficient water evaporation and clean freshwater collection. *J. Mater. Chem. A* **2019**, *7*, 11177–11185.
- [73] Wu, D. D.; Qu, D.; Jiang, W. S.; Chen, G.; An, L.; Zhuang, C. Q.; Sun, Z. C. Self-floating nanostructured Ni-NiO<sub>x</sub>/Ni foam for solar thermal water evaporation. *J. Mater. Chem. A* **2019**, *7*, 8485–8490.
- [74] Xu, Y.; Ma, J. X.; Han, Y.; Zhang, J. J.; Cui, F. Y.; Zhao, Y.; Li, X.; Wang, W. Multifunctional CuO nanowire mesh for highly efficient solar evaporation and water purification. *ACS Sustain. Chem. Eng.* **2019**, *7*, 5476–5485.
- [75] Cao, H. X.; Jiao, S. K.; Zhang, S.; Xu, J. G.; Wang, H. Y.; Guo, C. L. *In situ* synthesizing C-CuO composite for efficient photothermal conversion and its application in solar-driven interfacial evaporation. *Int. J. Energy Res.* **2021**, *45*, 7829–7839.
- [76] Wu, X.; Xu, J.; Chen, G. Y.; Fan, R.; Liu, X. K.; Xu, H. L. Harvesting, sensing and regulating light based on photo-thermal effect of Cu@CuO mesh. *Green Energy Environ.* **2017**, *2*, 387–392.
- [77] Cao, H. X.; Zhang, S.; Jiang, T.; Wang, D.; Zhu, Y. Y.; Bian, Z. T. Preparing photo-thermal conversion membrane with CuS-multi walled carbon nanotube (MWCNT) composite for solar-driven interfacial evaporation. *Mater. Lett.* **2022**, *317*, 132145.
- [78] Zhang, D.; Cai, Y. X.; Liang, Q. Q.; Wu, Z. T.; Sheng, N.; Zhang, M. H.; Wang, B. X.; Chen, S. Y. Scalable, flexible, durable, and salt-tolerant CuS/bacterial cellulose gel membranes for efficient interfacial solar evaporation. *ACS Sustain. Chem. Eng.* **2020**, *8*, 9017–9026.
- [79] Wu, X.; Robson, M. E.; Phelps, J. L.; Tan, J. S.; Shao, B.; Owens, G.; Xu, H. L. A flexible photothermal cotton-CuS nanocage-agarose aerogel towards portable solar steam generation. *Nano Energy* **2019**, *56*, 708–715.
- [80] Liu, H. X.; Yang, C. Y.; Guo, W.; Zhang, F.; Lin, H. M.; Zhao, L.; Ma, T. Y.; Lu, X. X.; Qu, F. Y. CoWO<sub>4-x</sub>-based photothermal membranes for solar-driven water evaporation and eutrophic lake water purification. *ACS Omega* **2020**, *5*, 31598–31607.
- [81] Zhang, X. Y.; Ren, L. P.; Xu, J.; Shang, B.; Liu, X.; Xu, W. L. Magnetically driven tunable 3D structured Fe<sub>3</sub>O<sub>4</sub> vertical array for high-performance solar steam generation. *Small* **2022**, *18*, 2105198.
- [82] He, J. X.; Liu, F.; Xiao, C. H.; Sun, H. X.; Li, J. Y.; Zhu, Z. Q.; Liang, W. D.; Li, A. Fe<sub>3</sub>O<sub>4</sub>/PPy-coated superhydrophilic polymer porous foam: A double layered photothermal material with a synergistic light-to-thermal conversion effect toward desalination. *Langmuir* **2021**, *37*, 12397–12408.
- [83] Zhang, B. P.; Gu, Q. F.; Wang, C.; Gao, Q. L.; Guo, J. X.; Wong, P. W.; Liu, C. T.; An, A. K. Self-assembled hydrophobic/hydrophilic porphyrin-Ti<sub>3</sub>C<sub>2</sub>T<sub>x</sub> MXene Janus membrane for dual-functional enabled photothermal desalination. *ACS Appl. Mater. Interfaces* **2021**, *13*, 3762–3770.
- [84] Wang, Z. G.; Yu, K.; Gong, S. J.; Mao, H. B.; Huang, R.; Zhu, Z. Q. Cu<sub>3</sub>BiS<sub>7</sub>/MXenes with excellent solar-thermal conversion for continuous and efficient seawater desalination. *ACS Appl. Mater. Interfaces* **2021**, *13*, 16246–16258.
- [85] Pu, L.; Ma, H. J.; Dong, J. C.; Zhang, C.; Lai, F. L.; He, G. J.; Ma, P. M.; Dong, W. F.; Huang, Y. P.; Liu, T. X. Xylem-inspired polyimide/MXene aerogels with radial lamellar architectures for highly sensitive strain detection and efficient solar steam generation. *Nano Lett.* **2022**, *22*, 4560–4568.
- [86] Mu, X. T.; Chen, L. H.; Qu, N. N.; Yu, J. L.; Jiang, X. Q.; Xiao, C. H.; Luo, X. P.; Hasi, Q. MXene/polypyrrole coated melamine-foam for efficient interfacial evaporation and photodegradation. *J. Colloid Interface Sci.* **2023**, *636*, 291–304.
- [87] Lu, Y.; Fan, D. Q.; Wang, Y. D.; Xu, H. L.; Lu, C. H.; Yang, X. F. Surface patterning of two-dimensional nanostructure-embedded photothermal hydrogels for high-yield solar steam generation. *ACS Nano* **2021**, *15*, 10366–10376.
- [88] Li, W.; Tian, X. H.; Li, X. F.; Liu, J.; Li, C. J.; Feng, X. Y.; Shu, C.; Yu, Z. Z. An environmental energy-enhanced solar steam

- evaporator derived from MXene-decorated cellulose acetate cigarette filter with ultrahigh solar steam generation efficiency. *J. Colloid Interface Sci.* **2022**, *606*, 748–757.
- [89] Chen, L. H.; Mu, X. T.; Guo, Y. P.; Lu, H. J.; Yang, Y. M.; Xiao, C. H.; Hasi, Q. MXene-doped kapok fiber aerogels with oleophobicity for efficient interfacial solar steam generation. *J. Colloid Interface Sci.* **2022**, *626*, 35–46.
- [90] Aizudin, M.; Krishna Sudha, M.; Goei, R.; Kuang Lua, S.; Poolamuri Pottammel, R.; Ling Yoong Tok, A.; Huixiang Ang, E. Sustainable production of molybdenum carbide (MXene) from fruit wastes for improved solar evaporation. *Chem. -Eur. J.* **2023**, *29*, e202203184.
- [91] Yu, F.; Ming, X.; Xu, Y.; Chen, Z. H.; Meng, D. X.; Cheng, H. Y.; Shi, Z. X.; Shen, P.; Wang, X. B. Quasimetallic molybdenum carbide-based flexible polyvinyl alcohol hydrogels for enhancing solar water evaporation. *Adv. Mater. Interfaces* **2019**, *6*, 1901168.
- [92] Zhu, L. L.; Gao, M. M.; Peh, C. K. N.; Wang, X. Q.; Ho, G. W. Self-contained monolithic carbon sponges for solar-driven interfacial water evaporation distillation and electricity generation. *Adv. Energy Mater.* **2018**, *8*, 1702149.
- [93] Zhou, J. G.; Sun, Z. L.; Chen, M. Q.; Wang, J. T.; Qiao, W. M.; Long, D. H.; Ling, L. C. Macroscopic and mechanically robust hollow carbon spheres with superior oil adsorption and light-to-heat evaporation properties. *Adv. Funct. Mater.* **2016**, *26*, 5368–5375.
- [94] Zhang, Z.; Feng, Z.; Qi, H.; Chen, Y. L.; Chen, Y. J.; Deng, Q. L.; Wang, S. Carbonized sorghum straw derived 3D cup-shaped evaporator with enhanced evaporation rate and energy efficiency. *Sustain. Mater. Technol.* **2022**, *32*, e00414.
- [95] Zhang, Y. D.; Deng, W. F.; Wu, M. Y.; Liu, Z. X.; Yu, G.; Cui, Q.; Liu, C.; Fatehi, P.; Li, B. Robust, scalable, and cost-effective surface carbonized pulp foam for highly efficient solar steam generation. *ACS Appl. Mater. Interfaces* **2023**, *15*, 7414–7426.
- [96] Zhang, W. M.; Yan, J.; Su, Q.; Han, J.; Gao, J. F. Hydrophobic and porous carbon nanofiber membrane for high performance solar-driven interfacial evaporation with excellent salt resistance. *J. Colloid Interface Sci.* **2022**, *612*, 66–75.
- [97] Yang, H. F.; Yang, G. C.; Qiao, Z. Q.; Bao, H. B.; Zhang, S. T.; Li, X. M.; Liu, Y. S. Facile deflagration synthesis of hollow carbon nanospheres with efficient performance for solar water evaporation. *ACS Appl. Mater. Interfaces* **2020**, *12*, 35193–35200.
- [98] Xiao, C. H.; Wang, S. S.; Guo, Y. P.; Zhang, Y. H.; Hasi, Q. M.; Tian, Q.; Chen, L. H. Coffee grounds-doped alginate porous materials for efficient solar steam generation. *Langmuir* **2022**, *38*, 1888–1896.
- [99] Tian, C.; Liu, J.; Ruan, R. F.; Tian, X. L.; Lai, X. Y.; Xing, L.; Su, Y. Q.; Huang, W.; Cao, Y.; Tu, J. C. Sandwich photothermal membrane with confined hierarchical carbon cells enabling high-efficiency solar steam generation. *Small* **2020**, *16*, 2000573.
- [100] Sun, P.; Zhang, W.; Zada, I.; Zhang, Y. X.; Gu, J. J.; Liu, Q. L.; Su, H. L.; Pantelić, D.; Jelenković, B.; Zhang, D. 3D-structured carbonized sunflower heads for improved energy efficiency in solar steam generation. *ACS Appl. Mater. Interfaces* **2020**, *12*, 2171–2179.
- [101] Ma, N.; Fu, Q.; Hong, Y. X.; Hao, X. Y.; Wang, X. G.; Ju, J.; Sun, J. L. Processing natural wood into an efficient and durable solar steam generation device. *ACS Appl. Mater. Interfaces* **2020**, *12*, 18165–18173.
- [102] Liu, F. Q. X.; Xia, L. M.; Zhang, L. Y.; Guo, F.; Zhang, X. X.; Yu, Y.; Yang, R. L. Sunflower-stalk-based solar-driven evaporator with a confined 2D water channel and an enclosed thermal-insulating cellular structure for stable and efficient steam generation. *ACS Appl. Mater. Interfaces* **2021**, *13*, 55299–55306.
- [103] Guan, W. X.; Guo, Y. H.; Yu, G. H. Carbon materials for solar water evaporation and desalination. *Small* **2021**, *17*, 2007176.
- [104] Fang, Q. L.; Li, T. T.; Chen, Z. M.; Lin, H. B.; Wang, P.; Liu, F. Full biomass-derived solar stills for robust and stable evaporation to collect clean water from various water-bearing media. *ACS Appl. Mater. Interfaces* **2019**, *11*, 10672–10679.
- [105] Liu, Y. M.; Chen, J. W.; Guo, D. W.; Cao, M. Y.; Jiang, L. Floatable, self-cleaning, and carbon-black-based superhydrophobic gauze for the solar evaporation enhancement at the air–water interface. *ACS Appl. Mater. Interfaces* **2015**, *7*, 13645–13652.
- [106] Wang, H. Q.; Lu, Z. C.; Ma, S. Y.; Li, Z. H.; Xin, Z. H.; Zhang, Z. H.; Zhou, B.; Shen, J.; Qin, L. L.; Du, A. Ultrablack poly(vinyl alcohol)-graphite composite xerogel with vertically arranged pores for highly efficient solar steam generation and desalination. *Adv. Energy Sustain. Res.* **2022**, *3*, 2100188.
- [107] Yin, Z.; Wang, H. M.; Jian, M. Q.; Li, Y. S.; Xia, K. L.; Zhang, M. C.; Wang, C. Y.; Wang, Q.; Ma, M.; Zheng, Q. S. et al. Extremely black vertically aligned carbon nanotube arrays for solar steam generation. *ACS Appl. Mater. Interfaces* **2017**, *9*, 28596–28603.
- [108] Wang, Y. C.; Zhang, L. B.; Wang, P. Self-floating carbon nanotube membrane on macroporous silica substrate for highly efficient solar-driven interfacial water evaporation. *ACS Sustain. Chem. Eng.* **2016**, *4*, 1223–1230.
- [109] Su, L. F.; Liu, X. Y.; Li, X.; Yang, B.; Wu, B.; Xia, R.; Qian, J. S.; Zhou, J. H.; Miao, L. Facile synthesis of vertically arranged CNTs for efficient solar-driven interfacial water evaporation. *ACS Omega* **2022**, *7*, 47349–47356.
- [110] Ma, X.; Fang, W. Z.; Guo, Y.; Li, Z. Y.; Chen, D. K.; Ying, W.; Xu, Z.; Gao, C.; Peng, X. S. Hierarchical porous SWCNT stringed carbon polyhedrons and PSS threaded MOF bilayer membrane for efficient solar vapor generation. *Small* **2019**, *15*, 1900354.
- [111] Liu, H. C.; Huang, G. C.; Wang, R.; Huang, L.; Wang, H. Z.; Hu, Y. Z.; Cong, G. T.; Bao, F.; Xu, M.; Zhu, C. Z. et al. Carbon nanotubes grown on the carbon fibers to enhance the photothermal conversion toward solar-driven applications. *ACS Appl. Mater. Interfaces* **2022**, *14*, 32404–32411.
- [112] Hu, N. N.; Zhao, S. L.; Chen, T. C.; Lu, X. N.; Zhang, J. L. Janus carbon nanotube@poly(butylene adipate-co-terephthalate) fabric for stable and efficient solar-driven interfacial evaporation. *ACS Appl. Mater. Interfaces* **2022**, *14*, 46010–46022.
- [113] Zhao, X.; Meng, X. T.; Zou, H. Q.; Wang, Z. H.; Du, Y. D.; Shao, Y.; Qi, J.; Qiu, J. S. Topographic manipulation of graphene oxide by polyaniline nanocone arrays enables high-performance solar-driven water evaporation. *Adv. Funct. Mater.* **2023**, *33*, 2209207.
- [114] Wang, X. Q.; Ou, G.; Wang, N.; Wu, H. Graphene-based recyclable photo-absorbers for high-efficiency seawater desalination. *ACS Appl. Mater. Interfaces* **2016**, *8*, 9194–9199.
- [115] Finnerty, C. T. K.; Menon, A. K.; Conway, K. M.; Lee, D.; Nelson, M.; Urban, J. J.; Sedlak, D.; Mi, B. X. Interfacial solar evaporation by a 3D graphene oxide stalk for highly concentrated brine treatment. *Environ. Sci. Technol.* **2021**, *55*, 15435–15445.
- [116] Yu, M. Y.; Li, C. J.; Li, W.; Min, P. Reduced graphene oxide decorated cellulose acetate filter evaporators for highly efficient water evaporation and purification driven by solar energy and environmental energy. *Adv. Sustain. Syst.* **2022**, *6*, 2200023.
- [117] Yan, S. W.; Song, H. J.; Li, Y.; Yang, J.; Jia, X. H.; Wang, S. Z.; Yang, X. F. Integrated reduced graphene oxide/polypyrrole hybrid aerogels for simultaneous photocatalytic decontamination and water evaporation. *Appl. Catal. B: Environ.* **2022**, *301*, 120820.
- [118] Li, Z. J.; Chen, D. K.; Gao, H.; Xie, H. Q.; Yu, W. Reduced graphene oxide composite nanowood for solar-driven interfacial evaporation and electricity generation. *Appl. Therm. Eng.* **2023**, *223*, 119985.
- [119] Li, C. J.; Li, W.; Zhao, H. Y.; Feng, X. Y.; Li, X. F.; Yu, Z. Z. Constructing central hollow cylindrical reduced graphene oxide foams with vertically and radially orientated porous channels for highly efficient solar-driven water evaporation and purification. *Nano Res.*, in press, <https://doi.org/10.1007/s12274-022-5348-5>.
- [120] Guo, A. K.; Ming, X.; Fu, Y.; Wang, G.; Wang, X. B. Fiber-based, double-sided, reduced graphene oxide films for efficient solar vapor generation. *ACS Appl. Mater. Interfaces* **2017**, *9*, 29958–29964.
- [121] Zou, Y.; Zhao, J. Y.; Zhu, J. Y.; Guo, X. Y.; Chen, P.; Duan, G. G.; Liu, X. H.; Li, Y. W. A mussel-inspired polydopamine-filled cellulose aerogel for solar-enabled water remediation. *ACS Appl. Mater. Interfaces* **2021**, *13*, 7617–7624.

- [122] Zhou, X. Y.; Zhao, F.; Guo, Y. H.; Rosenberger, B.; Yu, G. H. Architecting highly hydratable polymer networks to tune the water state for solar water purification. *Sci. Adv.* **2019**, *5*, eaaw5484.
- [123] Zhang, Y.; Yin, X. Y.; Yu, B.; Wang, X. L.; Guo, Q. Q.; Yang, J. Recyclable polydopamine-functionalized sponge for high-efficiency clean water generation with dual-purpose solar evaporation and contaminant adsorption. *ACS Appl. Mater. Interfaces* **2019**, *11*, 32559–32568.
- [124] Xu, Y.; Tang, C. Y.; Ma, J. X.; Liu, D. Q.; Qi, D. P.; You, S. J.; Cui, F. Y.; Wei, Y.; Wang, W. Low-tortuosity water microchannels boosting energy utilization for high water flux solar distillation. *Environ. Sci. Technol.* **2020**, *54*, 5150–5158.
- [125] Wilson, H. M.; Lim, H. W.; Lee, S. J. Highly efficient and salt-rejecting poly(vinyl alcohol) hydrogels with excellent mechanical strength for solar desalination. *ACS Appl. Mater. Interfaces* **2022**, *14*, 47800–47809.
- [126] Sun, S. J.; Wang, Y. M.; Sun, B. B.; Zhang, F. F.; Xu, Q.; Mi, H. Y.; Li, H.; Tao, X. M.; Guo, Z. H.; Liu, C. T. et al. Versatile Janus composite nonwoven solar absorbers with salt resistance for efficient wastewater purification and desalination. *ACS Appl. Mater. Interfaces* **2021**, *13*, 24945–24956.
- [127] Shi, Y.; Meng, N.; Wang, Y.; Cheng, Z. H.; Zhang, W. Y.; Liao, Y. Z. Scalable fabrication of conjugated microporous polymer sponges for efficient solar steam generation. *ACS Appl. Mater. Interfaces* **2022**, *14*, 4522–4531.
- [128] Qiao, L. F.; Li, N.; Luo, L.; He, J. T.; Lin, Y. X.; Li, J. J.; Yu, L. M.; Guo, C.; Murto, P.; Xu, X. F. Design of monolithic closed-cell polymer foams via controlled gas-foaming for high-performance solar-driven interfacial evaporation. *J. Mater. Chem. A* **2021**, *9*, 9692–9705.
- [129] Qi, D. P.; Liu, Y.; Liu, Y. B.; Liu, Z. Y.; Luo, Y. F.; Xu, H. B.; Zhou, X.; Zhang, J. J.; Yang, H.; Wang, W. et al. Polymeric membranes with selective solution-diffusion for intercepting volatile organic compounds during solar-driven water remediation. *Adv. Mater.* **2020**, *32*, 2004401.
- [130] Liu, Z. W.; Qing, R. K.; Xie, A. Q.; Liu, H.; Zhu, L. L.; Chen, S. Self-contained janus aerogel with antifouling and salt-rejecting properties for stable solar evaporation. *ACS Appl. Mater. Interfaces* **2021**, *13*, 18829–18837.
- [131] Liang, Y. Z.; Bai, Y. T.; Xie, A. Q.; Mao, J.; Zhu, L. L.; Chen, S. Solar-initiated frontal polymerization of photothermic hydrogels with high swelling properties for efficient water evaporation. *Sol. RRL* **2021**, *6*, 2100917.
- [132] Chen, Q. M.; Pei, Z. Q.; Xu, Y. S.; Li, Z.; Yang, Y.; Wei, Y.; Ji, Y. A durable monolithic polymer foam for efficient solar steam generation. *Chem. Sci.* **2018**, *9*, 623–628.
- [133] Guo, Y. H.; Zhao, X.; Zhao, F.; Jiao, Z. H.; Zhou, X. Y.; Yu, G. H. Tailoring surface wetting states for ultrafast solar-driven water evaporation. *Energy Environ. Sci.* **2020**, *13*, 2087–2095.
- [134] Guo, Y. H.; Zhao, F.; Zhou, X. Y.; Chen, Z. C.; Yu, G. H. Tailoring nanoscale surface topography of hydrogel for efficient solar vapor generation. *Nano Lett.* **2019**, *19*, 2530–2536.
- [135] Luo, Y. N.; Fu, B. W.; Shen, Q. C.; Hao, W.; Xu, J. L.; Min, M. D.; Liu, Y. M.; An, S.; Song, C. Y.; Tao, P. et al. Patterned surfaces for solar-driven interfacial evaporation. *ACS Appl. Mater. Interfaces* **2019**, *11*, 7584–7590.
- [136] Xu, Y.; Ma, J. X.; Liu, D. Q.; Xu, H. B.; Cui, F. Y.; Wang, W. Origami system for efficient solar driven distillation in emergency water supply. *Chem. Eng. J.* **2019**, *356*, 869–876.
- [137] Liu, H. J.; Liu, Y.; Wang, L. M.; Qin, X. H.; Yu, J. Y. Nanofiber based origami evaporator for multifunctional and omnidirectional solar steam generation. *Carbon* **2021**, *177*, 199–206.
- [138] Hong, S.; Shi, Y.; Li, R. Y.; Zhang, C. L.; Jin, Y.; Wang, P. Nature-inspired, 3D origami solar steam generator toward near full utilization of solar energy. *ACS Appl. Mater. Interfaces* **2018**, *10*, 28517–28524.
- [139] Zhu, M. W.; Li, Y. J.; Chen, G.; Jiang, F.; Yang, Z.; Luo, X. G.; Wang, Y. B.; Lacey, S. D.; Dai, J. Q.; Wang, C. W. et al. Tree-inspired design for high-efficiency water extraction. *Adv. Mater.* **2017**, *29*, 1704107.
- [140] Cui, T. T.; Liu, Z.; Gao, L. L.; He, Y. S.; Jin, B. W.; Meng, X.; Qi, Y. P.; Ye, C. H. Engineered wood with hierarchically tunable microchannels toward efficient solar vapor generation. *Langmuir* **2022**, *38*, 12773–12784.
- [141] Lu, J. L.; Ngo, C. V.; Singh, S. C.; Yang, J. J.; Xin, W.; Yu, Z.; Guo, C. L. Bioinspired hierarchical surfaces fabricated by femtosecond laser and hydrothermal method for water harvesting. *Langmuir* **2019**, *35*, 3562–3567.
- [142] Lei, W. W.; Khan, S.; Chen, L.; Suzuki, N.; Terashima, C.; Liu, K. S.; Fujishima, A.; Liu, M. J. Hierarchical structures hydrogel evaporator and superhydrophilic water collect device for efficient solar steam evaporation. *Nano Res.* **2021**, *14*, 1135–1140.
- [143] Wang, X.; Liu, Q. C.; Wu, S. Y.; Xu, B. X.; Xu, H. X. Multilayer polypyrrole nanosheets with self-organized surface structures for flexible and efficient solar-thermal energy conversion. *Adv. Mater.* **2019**, *31*, 1807716.
- [144] Gao, X.; Ren, H. Y.; Zhou, J. Y.; Du, R.; Yin, C.; Liu, R.; Peng, H. L.; Tong, L. M.; Liu, Z. F.; Zhang, J. Synthesis of hierarchical graphdiyne-based architecture for efficient solar steam generation. *Chem. Mater.* **2017**, *29*, 5777–5781.
- [145] Yao, H. Z.; Zhang, P. P.; Yang, C.; Liao, Q. H.; Hao, X. Z.; Huang, Y. X.; Zhang, M.; Wang, X. B.; Lin, T. Y.; Cheng, H. H. et al. Janus-interface engineering boosting solar steam towards high-efficiency water collection. *Energy Environ. Sci.* **2021**, *14*, 5330–5338.
- [146] Liao, Q. H.; Zhang, P. P.; Yao, H. Z.; Cheng, H. H.; Li, C.; Qu, L. T. Reduced graphene oxide-based spectrally selective absorber with an extremely low thermal emittance and high solar absorptance. *Adv. Sci.* **2020**, *7*, 1903125.
- [147] Zhou, L.; Zhuang, S. D.; He, C. Y.; Tan, Y. L.; Wang, Z. L.; Zhu, J. Self-assembled spectrum selective plasmonic absorbers with tunable bandwidth for solar energy conversion. *Nano Energy* **2017**, *32*, 195–200.
- [148] Ni, G.; Li, G.; Boriskina, S. V.; Li, H. X.; Yang, W. L.; Zhang, T. J.; Chen, G. Steam generation under one sun enabled by a floating structure with thermal concentration. *Nat. Energy* **2016**, *1*, 16126.
- [149] Ding, D. W.; Wu, H.; He, X. P.; Yang, F.; Gao, C. B.; Yin, Y. D.; Ding, S. J. A metal nanoparticle assembly with broadband absorption and suppressed thermal radiation for enhanced solar steam generation. *J. Mater. Chem. A* **2021**, *9*, 11241–11247.
- [150] Wang, F. Y.; Xu, N.; Zhao, W.; Zhou, L.; Zhu, P. C.; Wang, X. Y.; Zhu, B.; Zhu, J. A high-performing single-stage invert-structured solar water purifier through enhanced absorption and condensation. *Joule* **2021**, *5*, 1602–1612.
- [151] Gao, T.; Wang, Y. D.; Wu, X.; Wu, P.; Yang, X. F.; Li, Q.; Zhang, Z. Z.; Zhang, D. K.; Owens, G.; Xu, H. L. More from less: Improving solar steam generation by selectively removing a portion of evaporation surface. *Sci. Bull.* **2022**, *67*, 1572–1580.
- [152] Zhang, Z.; Mu, P.; He, J. X.; Zhu, Z. Q.; Sun, H. X.; Wei, H. J.; Liang, W. D.; Li, A. Facile and scalable fabrication of surface-modified sponge for efficient solar steam generation. *ChemSusChem* **2019**, *12*, 426–433.
- [153] Zhang, X. C.; Wang, X. N.; Wu, W. D.; Chen, X. D.; Wu, Z. X. Self-floating monodisperse microparticles with a nano-engineered surface composition and structure for highly efficient solar-driven water evaporation. *J. Mater. Chem. A* **2019**, *7*, 6963–6971.
- [154] Zeng, Y.; Yao, J. F.; Horri, B. A.; Wang, K.; Wu, Y. Z.; Li, D.; Wang, H. T. Solar evaporation enhancement using floating light-absorbing magnetic particles. *Energy Environ. Sci.* **2011**, *4*, 4074–4078.
- [155] Wang, C. J.; Wang, Y.; Yan, M. Y.; Zhang, W. X.; Wang, P.; Guan, W.; Zhang, S.; Yu, L. Y.; Feng, J. G.; Gan, Z. X. et al. Highly efficient self-floating jellyfish-like solar steam generators based on the partially carbonized enteromorpha aerogel. *J. Colloid Interface Sci.* **2023**, *630*, 297–305.
- [156] Li, H. R.; He, Y. R.; Hu, Y. W.; Wang, X. Z. Commercially available activated carbon fiber felt enables efficient solar steam generation. *ACS Appl. Mater. Interfaces* **2018**, *10*, 9362–9368.

- [157] Jin, M. T.; Wu, Z. T.; Guan, F. Y.; Zhang, D.; Wang, B. X.; Sheng, N.; Qu, X. Y.; Deng, L. L.; Chen, S. Y.; Chen, Y. et al. Hierarchically designed three-dimensional composite structure on a cellulose-based solar steam generator. *ACS Appl. Mater. Interfaces* **2022**, *14*, 12284–12294.
- [158] Chen, Y. X.; Shi, Y. M.; Kou, H.; Liu, D. L.; Huang, Y.; Chen, Z. G.; Zhang, B. Self-floating carbonized tissue membrane derived from commercial facial tissue for highly efficient solar steam generation. *ACS Sustain. Chem. Eng.* **2019**, *7*, 2911–2915.
- [159] Ge, B.; Han, B. B.; Lv, J.; Zhao, L. M.; Yin, Y. B.; Ren, G. N.; Zhang, Z. Z. Design of self-floating photothermal conversion devices with solar steam generation capability. *Adv. Mater. Interfaces* **2022**, *9*, 2101357.
- [160] Wang, C. J.; Wang, Y.; Guan, W.; Wang, P.; Feng, J. G.; Song, N.; Dong, H. Z.; Yu, L. Y.; Sui, L. N.; Gan, Z. X. et al. A self-floating and integrated bionic mushroom for highly efficient solar steam generation. *J. Colloid Interface Sci.* **2022**, *612*, 88–96.
- [161] Chen, J. X.; Li, B.; Hu, G. X.; Aleisa, R.; Lei, S.; Yang, F.; Liu, D. L.; Lyu, F. L.; Wang, M. Z.; Ge, X. W. et al. Integrated evaporator for efficient solar-driven interfacial steam generation. *Nano Lett.* **2020**, *20*, 6051–6058.
- [162] Chen, G. Y.; Sun, J. M.; Peng, Q.; Sun, Q.; Wang, G.; Cai, Y. J.; Gu, X. G.; Shuai, Z. G.; Tang, B. Z. Biradical-featured stable organic-small-molecule photothermal materials for highly efficient solar-driven water evaporation. *Adv. Mater.* **2020**, *32*, 1908537.
- [163] Zhang, F. Y.; Li, Y. G.; Bai, X. H.; Wang, S. F.; Liang, B. L.; Fu, G. S.; Wu, Z. S. Synthesis of mesoporous Fe<sub>3</sub>Si aerogel as a photothermal material for highly efficient and stable corrosive-water evaporation. *J. Mater. Chem. A* **2018**, *6*, 23263–23269.
- [164] Liu, H. J.; Alam, K.; He, M. T.; Liu, Y.; Wang, L. M.; Qin, X. H.; Yu, J. Y. Sustainable cellulose aerogel from waste cotton fabric for high-performance solar steam generation. *ACS Appl. Mater. Interfaces* **2021**, *13*, 49860–49867.
- [165] Li, H. X.; Wen, H. F.; Li, J.; Huang, J. C.; Wang, D.; Tang, B. Z. Doping AIE photothermal molecule into all-fiber aerogel with self-pumping water function for efficiency solar steam generation. *ACS Appl. Mater. Interfaces* **2020**, *12*, 26033–26040.
- [166] Jiang, F.; Liu, H.; Li, Y. J.; Kuang, Y. D.; Xu, X.; Chen, C. J.; Huang, H.; Jia, C.; Zhao, X. P.; Hitz, E. et al. Lightweight, mesoporous, and highly absorptive all-nanofiber aerogel for efficient solar steam generation. *ACS Appl. Mater. Interfaces* **2018**, *10*, 1104–1112.
- [167] Tian, S.; Huang, Z. M.; Tan, J. H.; Cui, X.; Xiao, Y. F.; Wan, Y. P.; Li, X. Z.; Zhao, Q.; Li, S. L.; Lee, C. S. Manipulating interfacial charge-transfer absorption of cocrystal absorber for efficient solar seawater desalination and water purification. *ACS Energy Lett.* **2020**, *5*, 2698–2705.
- [168] Chang, C.; Tao, P.; Fu, B. W.; Xu, J. L.; Song, C. Y.; Wu, J. B.; Shang, W.; Deng, T. Three-dimensional porous solar-driven interfacial evaporator for high-efficiency steam generation under low solar flux. *ACS Omega* **2019**, *4*, 3546–3555.
- [169] Peng, F. J.; Xu, J.; Bai, X. L.; Feng, G. P.; Zeng, X. H.; Ibn Raihan, R.; Bao, H. F. A Janus solar evaporator with 2D water path for highly efficient salt-resisting solar steam generation. *Sol. Energy Mater. Sol. Cells* **2021**, *221*, 110910.
- [170] Li, X. Q.; Xu, W. C.; Tang, M. Y.; Zhou, L.; Zhu, B.; Zhu, S. N.; Zhu, J. Graphene oxide-based efficient and scalable solar desalination under one sun with a confined 2D water path. *Proc. Natl. Acad. Sci. USA* **2016**, *113*, 13953–13958.
- [171] Wang, Y. D.; Wu, X.; Wu, P.; Yu, H. M.; Zhao, J. Y.; Yang, X. F.; Li, Q.; Zhang, Z. Z.; Zhang, D. K.; Owens, G. et al. Salt isolation from waste brine enabled by interfacial solar evaporation with zero liquid discharge. *J. Mater. Chem. A* **2022**, *10*, 14470–14478.
- [172] Chen, J. X.; Feng, J.; Li, Z. W.; Xu, P. P.; Wang, X. J.; Yin, W. W.; Wang, M. Z.; Ge, X. W.; Yin, Y. D. Space-confined seeded growth of black silver nanostructures for solar steam generation. *Nano Lett.* **2019**, *19*, 400–407.
- [173] Zhang, Z. Y.; Liu, H. Y.; Kong, Z.; Fang, M. W.; Wang, M. L.; Zhu, Y. Mushroom-like graphene nanosheets/copper sulfide nanowires foam with Janus-type wettability for solar steam generation. *ACS Appl. Nano Mater.* **2022**, *5*, 4931–4937.
- [174] Xu, N.; Hu, X. Z.; Xu, W. C.; Li, X. Q.; Zhou, L.; Zhu, S. N.; Zhu, J. Mushrooms as efficient solar steam-generation devices. *Adv. Mater.* **2017**, *29*, 1606762.
- [175] Menon, A. K.; Haechler, I.; Kaur, S.; Lubner, S.; Prasher, R. S. Enhanced solar evaporation using a photo-thermal umbrella for wastewater management. *Nat. Sustain.* **2020**, *3*, 144–151.
- [176] Ma, X. L.; Jia, X. D.; Yao, G. C.; Wen, D. S. Umbrella evaporator for continuous solar vapor generation and salt harvesting from seawater. *Cell Rep. Phys. Sci.* **2022**, *3*, 100940.
- [177] Li, X. Q.; Lin, R. X.; Ni, G.; Xu, N.; Hu, X. Z.; Zhu, B.; Lv, G. X.; Li, J. L.; Zhu, S. N.; Zhu, J. Three-dimensional artificial transpiration for efficient solar waste-water treatment. *Natl. Sci. Rev.* **2018**, *5*, 70–77.
- [178] Xia, Y.; Hou, Q. F.; Jubaer, H.; Li, Y.; Kang, Y.; Yuan, S.; Liu, H. Y.; Woo, M. W.; Zhang, L.; Gao, L. et al. Spatially isolating salt crystallisation from water evaporation for continuous solar steam generation and salt harvesting. *Energy Environ. Sci.* **2019**, *12*, 1840–1847.
- [179] Li, X. Q.; Li, J. L.; Lu, J. Y.; Xu, N.; Chen, C. L.; Min, X. Z.; Zhu, B.; Li, H. X.; Zhou, L.; Zhu, S. N. et al. Enhancement of interfacial solar vapor generation by environmental energy. *Joule* **2018**, *2*, 1331–1338.
- [180] Zhao, H. Y.; Huang, J.; Zhou, J.; Chen, L. F.; Wang, C. M.; Bai, Y. X.; Zhou, J.; Deng, Y.; Dong, W. X.; Li, Y. S. et al. Biomimetic design of macroporous 3D truss materials for efficient interfacial solar steam generation. *ACS Nano* **2022**, *16*, 3554–3562.
- [181] Yuan, B. H.; Zhang, C. F.; Liang, Y.; Yang, L. X.; Yang, H. W.; Bai, L. J.; Wei, D. L.; Wang, W. X.; Wang, Q. Y.; Chen, H. A low-cost 3D spherical evaporator with unique surface topology and inner structure for solar water evaporation-assisted dye wastewater treatment. *Adv. Sustain. Syst.* **2021**, *5*, 2000245.
- [182] Yu, Z.; Cheng, S. A.; Li, C. C.; Li, L. X.; Yang, J. W. Highly efficient solar vapor generator enabled by a 3D hierarchical structure constructed with hydrophilic carbon felt for desalination and wastewater treatment. *ACS Appl. Mater. Interfaces* **2019**, *11*, 32038–32045.
- [183] Yang, K. J.; Pan, T. T.; Dang, S. C.; Gan, Q. Q.; Han, Y. Three-dimensional open architecture enabling salt-rejection solar evaporators with boosted water production efficiency. *Nat. Commun.* **2022**, *13*, 6653.
- [184] Wang, Y. C.; Sun, X. Y.; Tao, S. Y. Rational 3D coiled morphology for efficient solar-driven desalination. *Environ. Sci. Technol.* **2020**, *54*, 16240–16248.
- [185] Tu, C.; Cai, W. F.; Chen, X.; Ouyang, X. L.; Zhang, H.; Zhang, Z. A 3D-structured sustainable solar-driven steam generator using super-black nylon flocking materials. *Small* **2019**, *15*, 1902070.
- [186] Ni, F.; Xiao, P.; Zhang, C.; Liang, Y.; Gu, J. C.; Zhang, L.; Chen, T. Micro-/macroscopically synergetic control of switchable 2D/3D photothermal water purification enabled by robust, portable, and cost-effective cellulose papers. *ACS Appl. Mater. Interfaces* **2019**, *11*, 15498–15506.
- [187] Liu, H.; Ye, H. G.; Gao, M. M.; Li, Q.; Liu, Z. W.; Xie, A. Q.; Zhu, L. L.; Ho, G. W.; Chen, S. Conformal microfluidic-blow-spun 3D photothermal catalytic spherical evaporator for omnidirectional enhanced solar steam generation and CO<sub>2</sub> reduction. *Adv. Sci.* **2021**, *8*, 2101232.
- [188] Liang, Y. Z.; Guo, J. C.; Li, J. J.; Mao, J.; Xie, A. Q.; Zhu, L. L.; Chen, S. Robust and flexible 3D photothermal evaporator with heat storage for high-performance solar-driven evaporation. *Adv. Sustain. Syst.* **2022**, *6*, 2200236.
- [189] Chen, G. L.; Zhang, N.; Li, N.; Yu, L. M.; Xu, X. F. A 3D hemispheric steam generator based on an organic-inorganic composite light absorber for efficient solar evaporation and desalination. *Adv. Mater. Interfaces* **2020**, *7*, 1901715.
- [190] Wu, P.; Wu, X.; Wang, Y. D.; Xu, H. L.; Owens, G. Towards

- sustainable saline agriculture: Interfacial solar evaporation for simultaneous seawater desalination and saline soil remediation. *Water Res.* **2022**, *212*, 118099.
- [191] Wu, L.; Dong, Z. C.; Cai, Z. R.; Ganapathy, T.; Fang, N. X.; Li, C. X.; Yu, C. L.; Zhang, Y.; Song, Y. L. Highly efficient three-dimensional solar evaporator for high salinity desalination by localized crystallization. *Nat. Commun.* **2020**, *11*, 521.
- [192] Gao, T.; Wu, X.; Wang, Y. D.; Owens, G.; Xu, H. L. A hollow and compressible 3D photothermal evaporator for highly efficient solar steam generation without energy loss. *Sol. RRL* **2021**, *5*, 2100053.
- [193] Xu, Z. C.; Ran, X. Q.; Wang, D.; Zhong, M. F.; Zhang, Z. J. High efficient 3D solar interfacial evaporator: Achieved by the synergy of simple material and structure. *Desalination* **2022**, *525*, 115495.
- [194] Gao, T.; Wu, X.; Owens, G.; Xu, H. L. A cobalt oxide@polydopamine-reduced graphene oxide-based 3D photothermal evaporator for highly efficient solar steam generation. *Tungsten* **2020**, *2*, 423–432.
- [195] Wu, P.; Wu, X.; Wang, Y. D.; Xu, H. L.; Owens, G. A biomimetic interfacial solar evaporator for heavy metal soil remediation. *Chem. Eng. J.* **2022**, *435*, 134793.
- [196] Shao, B.; Wu, X.; Wang, Y. D.; Gao, T.; Liu, Z. Q.; Owens, G.; Xu, H. L. A general method for selectively coating photothermal materials on 3D porous substrate surfaces towards cost-effective and highly efficient solar steam generation. *J. Mater. Chem. A* **2020**, *8*, 24703–24709.
- [197] Khajevand, M.; Azizian, S.; Jaleh, B. A bio-based 3D evaporator nanocomposite for highly efficient solar desalination. *Sep. Purif. Technol.* **2022**, *284*, 102078.
- [198] Shi, Y.; Zhang, C. L.; Li, R. Y.; Zhuo, S. F.; Jin, Y.; Shi, L.; Hong, S.; Chang, J.; Ong, C.; Wang, P. Solar evaporator with controlled salt precipitation for zero liquid discharge desalination. *Environ. Sci. Technol.* **2018**, *52*, 11822–11830.
- [199] Li, R. Y.; Wu, M. C.; Aleid, S.; Zhang, C. L.; Wang, W. B.; Wang, P. An integrated solar-driven system produces electricity with fresh water and crops in arid regions. *Cell Rep. Phys. Sci.* **2022**, *3*, 100781.
- [200] Zhang, C. L.; Shi, Y.; Shi, L.; Li, H. X.; Li, R. Y.; Hong, S.; Zhuo, S. F.; Zhang, T. J.; Wang, P. Designing a next generation solar crystallizer for real seawater brine treatment with zero liquid discharge. *Nat. Commun.* **2021**, *12*, 998.
- [201] Bian, Y.; Shen, Y.; Tang, K.; Du, Q. Q.; Hao, L. C.; Liu, D. Y.; Hao, J. G.; Zhou, D.; Wang, X. K.; Zhang, H. L. et al. Carbonized tree-like furry magnolia fruit-based evaporator replicating the feat of plant transpiration. *Glob. Chall.* **2019**, *3*, 1900040.
- [202] Wu, X.; Wu, Z. Q.; Wang, Y. D.; Gao, T.; Li, Q.; Xu, H. L. All-cold evaporation under one sun with zero energy loss by using a heatsink inspired solar evaporator. *Adv. Sci.* **2021**, *8*, 2002501.
- [203] Wu, X.; Gao, T.; Han, C. H.; Xu, J. S.; Owens, G.; Xu, H. L. A photothermal reservoir for highly efficient solar steam generation without bulk water. *Sci. Bull.* **2019**, *64*, 1625–1633.
- [204] Song, H. M.; Liu, Y. H.; Liu, Z. J.; Singer, M. H.; Li, C. Y.; Cheney, A. R.; Ji, D. X.; Zhou, L.; Zhang, N.; Zeng, X. et al. Cold vapor generation beyond the input solar energy limit. *Adv. Sci.* **2018**, *5*, 1800222.
- [205] Wang, Y. D.; Wu, X.; Yang, X. F.; Owens, G.; Xu, H. L. Reversing heat conduction loss: Extracting energy from bulk water to enhance solar steam generation. *Nano Energy* **2020**, *78*, 105269.
- [206] Chen, J. X.; Lee, M.; Qiu, Y. H.; Wu, C. L. M.; Li, B.; Yin, Y. D. Emulsion-templated synthesis of 3D evaporators for efficient solar steam generation. *SmartMat* **2023**, *4*, e1140.
- [207] Wang, Y. D.; Wu, X.; Wu, P.; Zhao, J. Y.; Yang, X. F.; Owens, G.; Xu, H. L. Enhancing solar steam generation using a highly thermally conductive evaporator support. *Sci. Bull.* **2021**, *66*, 2479–2488.
- [208] Li, J. L.; Wang, X. Y.; Lin, Z. H.; Xu, N.; Li, X. Q.; Liang, J.; Zhao, W.; Lin, R. X.; Zhu, B.; Liu, G. L. et al. Over 10 kg·m<sup>-2</sup>·h<sup>-1</sup> evaporation rate enabled by a 3D interconnected porous carbon foam. *Joule* **2020**, *4*, 928–937.
- [209] Wang, H. Q.; Zhang, C.; Ji, X. J.; Yang, J. M.; Zhang, Z. H.; Ma, Y.; Zhang, Z. H.; Zhou, B.; Shen, J.; Du, A. Over 11 kg·m<sup>-2</sup>·h<sup>-1</sup> evaporation rate achieved by cooling metal-organic framework foam with pine needle-like hierarchical structures to subambient temperature. *ACS Appl. Mater. Interfaces* **2022**, *14*, 10257–10266.
- [210] Wang, Y. D.; Wu, X.; Gao, T.; Lu, Y.; Yang, X. F.; Chen, G. Y.; Owens, G.; Xu, H. L. Same materials, bigger output: A reversibly transformable 2D-3D photothermal evaporator for highly efficient solar steam generation. *Nano Energy* **2021**, *79*, 105477.
- [211] Chen, Y. Q.; Wang, Y. D.; Xu, J.; Ibn Raihan, R.; Guo, B.; Yang, G.; Li, M. Y.; Bao, H. F.; Xu, H. L. A 3D opened hollow photothermal evaporator for highly efficient solar steam generation. *Sol. RRL* **2022**, *6*, 2200202.
- [212] Yin, K.; Wu, Z. P.; Wu, J. R.; Zhu, Z.; Zhang, F.; Duan, J. A. Solar-driven thermal-wind synergistic effect on laser-textured superhydrophilic copper foam architectures for ultrahigh efficient vapor generation. *Appl. Phys. Lett.* **2021**, *118*, 211905.
- [213] Wang, Y. D.; Wu, X.; Shao, B.; Yang, X. F.; Owens, G.; Xu, H. L. Boosting solar steam generation by structure enhanced energy management. *Sci. Bull.* **2020**, *65*, 1380–1388.
- [214] Xu, N.; Zhu, P. C.; Sheng, Y.; Zhou, L.; Li, X. Q.; Tan, H. R.; Zhu, S. N.; Zhu, J. Synergistic tandem solar electricity-water generators. *Joule* **2020**, *4*, 347–358.
- [215] Zhou, X. Y.; Zhao, F.; Zhang, P. P.; Yu, G. H. Solar water evaporation toward water purification and beyond. *ACS Mater. Lett.* **2021**, *3*, 1112–1129.
- [216] Zhou, X. Y.; Guo, Y. H.; Zhao, F.; Yu, G. H. Hydrogels as an emerging material platform for solar water purification. *Acc. Chem. Res.* **2019**, *52*, 3244–3253.
- [217] Zhou, X. Y.; Guo, Y. H.; Zhao, F.; Shi, W.; Yu, G. H. Topology-controlled hydration of polymer network in hydrogels for solar-driven wastewater treatment. *Adv. Mater.* **2020**, *32*, 2007012.
- [218] Zhao, F.; Zhou, X. Y.; Shi, Y.; Qian, X.; Alexander, M.; Zhao, X. P.; Mendez, S.; Yang, R. G.; Qu, L. T.; Yu, G. H. Highly efficient solar vapour generation via hierarchically nanostructured gels. *Nat. Nanotechnol.* **2018**, *13*, 489–495.
- [219] Zhao, F.; Guo, Y. H.; Zhou, X. Y.; Shi, W.; Yu, G. H. Materials for solar-powered water evaporation. *Nat. Rev. Mater.* **2020**, *5*, 388–401.
- [220] Zhang, P. P.; Zhao, F.; Shi, W.; Lu, H. Y.; Zhou, X. Y.; Guo, Y. H.; Yu, G. H. Super water-extracting gels for solar-powered volatile organic compounds management in the hydrological cycle. *Adv. Mater.* **2022**, *34*, 2110548.
- [221] Guo, Y. H.; Zhou, X. Y.; Zhao, F.; Bae, J.; Rosenberger, B.; Yu, G. H. Synergistic energy nanoconfinement and water activation in hydrogels for efficient solar water desalination. *ACS Nano* **2019**, *13*, 7913–7919.
- [222] Guo, Y. H.; Lu, H. Y.; Zhao, F.; Zhou, X. Y.; Shi, W.; Yu, G. H. Biomass-derived hybrid hydrogel evaporators for cost-effective solar water purification. *Adv. Mater.* **2020**, *32*, 1907061.
- [223] Guo, Y. H.; de Vasconcelos, L. S.; Manohar, N.; Geng, J. F.; Johnston, K. P.; Yu, G. H. Highly elastic interconnected porous hydrogels through self-assembled templating for solar water purification. *Angew. Chem., Int. Ed.* **2022**, *61*, e202114074.
- [224] Guo, Y. H.; Bae, J.; Fang, Z. W.; Li, P. P.; Zhao, F.; Yu, G. H. Hydrogels and hydrogel-derived materials for energy and water sustainability. *Chem. Rev.* **2020**, *120*, 7642–7707.
- [225] Zou, H. Q.; Meng, X. T.; Zhao, X.; Qiu, J. S. Hofmeister effect-enhanced hydration chemistry of hydrogel for high-efficiency solar-driven interfacial desalination. *Adv. Mater.* **2023**, *35*, 2207262.
- [226] Yin, X. Y.; Zhang, Y.; Guo, Q. Q.; Cai, X. B.; Xiao, J. F.; Ding, Z. F.; Yang, J. Macroporous double-network hydrogel for high-efficiency solar steam generation under 1 sun illumination. *ACS Appl. Mater. Interfaces* **2018**, *10*, 10998–11007.
- [227] Liang, X. C.; Zhang, X. J.; Huang, Q. C.; Zhang, H.; Liu, C. K.; Liu, Y. Z. Simple preparation of external-shape and internal-channel size adjustable porous hydrogels by fermentation for efficient solar interfacial evaporation. *Sol. Energy* **2020**, *208*, 778–786.

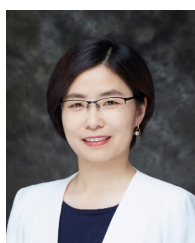
- [228] Gui, Z. Y.; Xiang, D. P. Hierarchically designed evaporators with dual-layered hydrogel/aerogel structure for efficient solar water evaporation. *Sep. Purif. Technol.* **2023**, *310*, 123237.
- [229] Chen, X. X.; Wu, Z. Y.; Lai, D. G.; Zheng, M.; Xu, L.; Huo, J. B.; Chen, Z. X.; Yuan, B. L.; Fu, M. L. Resilient biomass-derived hydrogel with tailored topography for highly efficient and long-term solar evaporation of high-salinity brine. *J. Mater. Chem. A* **2020**, *8*, 22645–22656.
- [230] Guo, Y. H.; Yu, G. H. Engineering hydrogels for efficient solar desalination and water purification. *Acc. Mater. Res.* **2021**, *2*, 374–384.
- [231] Guo, Y. H.; Fang, Z. W.; Yu, G. H. Multifunctional hydrogels for sustainable energy and environment. *Polym. Int.* **2021**, *70*, 1425–1432.
- [232] Lei, C. X.; Guo, Y. H.; Guan, W. X.; Yu, G. H. Polymeric materials for solar water purification. *J. Polym. Sci.* **2021**, *59*, 3084–3099.
- [233] Guan, Q. F.; Han, Z. M.; Ling, Z. C.; Yang, H. B.; Yu, S. H. Sustainable wood-based hierarchical solar steam generator: A biomimetic design with reduced vaporization enthalpy of water. *Nano Lett.* **2020**, *20*, 5699–5704.
- [234] Ma, Q. L.; Yin, P. F.; Zhao, M. T.; Luo, Z. Y.; Huang, Y.; He, Q. Y.; Yu, Y. F.; Liu, Z. Q.; Hu, Z. N.; Chen, B. et al. MOF-based hierarchical structures for solar-thermal clean water production. *Adv. Mater.* **2019**, *31*, 1808249.
- [235] Yan, X. L.; Lyu, S. Z.; Xu, X. Q.; Chen, W. B.; Shang, P. N.; Yang, Z. F.; Zhang, G.; Chen, W. H.; Wang, Y. P.; Chen, L. Superhydrophilic 2D covalent organic frameworks as broadband absorbers for efficient solar steam generation. *Angew. Chem., Int. Ed.* **2022**, *61*, e202201900.
- [236] Li, C. X.; Cao, S. J.; Lutzki, J.; Yang, J.; Konegger, T.; Kleitz, F.; Thomas, A. A covalent organic framework/graphene dual-region hydrogel for enhanced solar-driven water generation. *J. Am. Chem. Soc.* **2022**, *144*, 3083–3090.
- [237] Zhu, F. B.; Wang, L. Q.; Demir, B.; An, M.; Wu, Z. L.; Yin, J.; Xiao, R.; Zheng, Q.; Qian, J. Accelerating solar desalination in brine through ion activated hierarchically porous polyion complex hydrogels. *Mater. Horiz.* **2020**, *7*, 3187–3195.
- [238] Zhou, X. Y.; Zhao, F.; Guo, Y. H.; Zhang, Y.; Yu, G. H. A hydrogel-based antifouling solar evaporator for highly efficient water desalination. *Energy Environ. Sci.* **2018**, *11*, 1985–1992.



**Yida Wang** is currently a Postdoctoral Research Fellow at the Department of Chemistry, Tsinghua University. He received his Ph.D. degree at the University of South Australia in 2022 under the supervision of Prof. Haolan Xu. His research interest focuses on carbon- and fiber-based materials for solar energy conversion, thermal energy management, and relevant healthcare and sustainable applications. He has authored more than 30 journal papers, including 10 ESI highly cited papers.



**Li Yu** received his Ph.D. degree from Future Industries Institute, University of South Australia in 2016. Then he conducted his postdoctoral research at Shenzhen University. He was promoted to Associate Professor in 2020. Currently, he works in College of Health Science and Environmental Engineering, Shenzhen Technology University. His research interests include nanomaterials, polyelectrolytes, polyelectrolyte multilayers, surface coatings, and their functionalities in water purification.



**Yingying Zhang** received her Ph.D. degree in physical chemistry from Peking University in 2007. From June 2008 to June 2011, she worked in Los Alamos National Laboratory as a postdoctoral research associate. She joined Tsinghua University in July of 2011 and currently is a tenured professor in the Department of Chemistry. Her research focuses on the design and controlled preparation of nanocarbon, silk, and their hybrid materials, aiming to develop high performance flexible electronics and wearable systems. She has authored 150 journal papers with over 10,000 citations. Besides, she serves as the topic editor of *Accounts of Materials Research* and on the board of *Matter*, *Science Bulletin*, *Cell Reports Physical Science*, and *Advanced Materials Technologies*, etc.



**Haolan Xu** is a Professor at Future Industries Institute, the University of South Australia. He obtained his Ph.D. degree at Shanghai Institute of Ceramics, Chinese Academy of Sciences in 2008. Then he worked at Max Planck Institute of Colloids and Interfaces as an Alexander von Humboldt Postdoctoral Fellow. He joined the University of South Australia in January 2011. His research interests include colloid and interface physical chemistry, catalysis, and solar-thermal energy conversion and applications.